



1 **The Fifth International Workshop on Ice Nucleation Phase 3**  
2 **(FIN-03): Field Intercomparison of Ice Nucleation**  
3 **Measurements**

4  
5 Paul J. DeMott<sup>1</sup>, Jessica A. Mirrielees<sup>2,a</sup>, Sarah Suda Petters<sup>3,b</sup>, Daniel J. Cziczo<sup>4,c</sup>, Markus D.  
6 Petters<sup>3,b</sup>, Heinz G. Bingemer<sup>5</sup>, Thomas C. J. Hill<sup>1</sup>, Karl Froyd<sup>6,7,d</sup>, Sarvesh Garimella<sup>4,e</sup>, A.  
7 Gannet Hallar<sup>8,9</sup>, Ezra J.T. Levin<sup>1,f</sup>, Ian B. McCubbin<sup>8,9</sup>, Anne E. Perring<sup>6,7,g</sup>, Christopher N.  
8 Rapp<sup>c</sup>, Thea Schiebel<sup>10,h</sup>, Jann Schrod<sup>5</sup>, Kaitlyn J. Suski<sup>1,i</sup>, Daniel Weber<sup>5,j</sup>, Martin J. Wolf<sup>4,k</sup>,  
9 Maria Zawadowicz<sup>4,l</sup>, Jake Zenker<sup>2,m</sup>, Ottmar Möhler<sup>10</sup> and Sarah D. Brooks<sup>2</sup>

10  
11 <sup>1</sup>Department of Atmospheric Science, Colorado State University, Fort Collins, CO, USA

12 <sup>2</sup>Department of Atmospheric Sciences, Texas A&M University, College Station, TX, USA

13 <sup>3</sup>Department of Marine, Earth and Atmospheric Sciences, North Carolina State University,  
14 Raleigh, NC, USA

15 <sup>4</sup>Department of Earth, Atmospheric and Planetary Sciences, Massachusetts Institute of  
16 Technology, Cambridge, MA, USA

17 <sup>5</sup>Institute for Atmospheric and Environmental Sciences, Goethe University Frankfurt, 60438  
18 Frankfurt am Main, Germany

19 <sup>6</sup>NOAA Earth System Research Laboratory, Boulder, CO, USA

20 <sup>7</sup>CIRES, University of Colorado, Boulder, CO, USA

21 <sup>8</sup>Storm Peak Laboratory, Department of Atmospheric Sciences, University of Utah, Salt Lake  
22 City, Utah, USA

23 <sup>9</sup>Department of Atmospheric Sciences, University of Utah, Salt Lake City, Utah, USA

24 <sup>10</sup>Institute of Meteorology and Climate Research (IMK-AAF), Karlsruhe Institute of Technology  
25 (KIT), Eggenstein-Leopoldshafen, Germany

26 <sup>a</sup>now at: Chemistry Department, University of Michigan, Ann Arbor, MI

27 <sup>b</sup>now at: College of Engineering Center for Environmental Research and Technology (CE-  
28 CERT); Department of Chemical and Environmental Engineering, University of California  
29 Riverside, Riverside, CA

30 <sup>c</sup>now at: Department of Earth, Atmospheric, and Planetary Sciences, Purdue University, West  
31 Lafayette, IN, USA

32 <sup>d</sup>now at: Air Innova, Boulder, CO, USA

33 <sup>e</sup>now at: ACME AtronOmatic, LLC, Portland, OR, USA

34 <sup>f</sup>now at: Colorado Department of Public Health and Environment, Denver CO, USA

35 <sup>g</sup>now at: Department of Chemistry, Colgate University, Hamilton, NY, USA

36 <sup>h</sup>now at: Faculty 8- Mathematics and Physics, University of Stuttgart, Stuttgart, Germany

37 <sup>i</sup>now at: Rainmaker Technology Corporation, El Segundo, CA, USA

38 <sup>j</sup>now at: Federal Waterways Engineering and Research Institute, Karlsruhe, Germany

39 <sup>k</sup>now at: Yale Center for Law and Policy, New Haven, CT, USA

40 <sup>l</sup>now at: Brookhaven National Laboratory, Richland, WA, USA

41 <sup>m</sup>now at: Sandia National Laboratories, Albuquerque, NM, USA

42 Correspondence: Paul J. DeMott ([Paul.Demott@colostate.edu](mailto:Paul.Demott@colostate.edu))

43



#### 44 **Abstract**

45           The third phase of the Fifth International Ice Nucleation Workshop (FIN-03) was  
46 conducted at Storm Peak Laboratory in Steamboat Springs, Colorado in September 2015 to  
47 facilitate the intercomparison of instruments measuring ice nucleating particles (INPs) in the  
48 field. Instruments included a subset of two online and four offline measurement systems for  
49 INPs, a subset of those utilized in the laboratory study that comprised the second phase of FIN  
50 (FIN-02). Composition of total aerosols were characterized by the Particle Ablation by Laser  
51 Mass Spectrometry (PALMS) and Wideband Integrated Bioaerosol Sensor (WIBS) instruments,  
52 and aerosol size distributions were measured by a Laser Aerosol Spectrometer (LAS). The  
53 dominant total particle compositions present during FIN-03 were composed of sulfates, organic  
54 compounds, and nitrates, as well as particles derived from biomass burning. Mineral dust  
55 containing particle types were ubiquitous throughout and represented 67% of supermicron  
56 particles. Total WIBS fluorescing particle concentrations for particles with diameter  $> 0.5 \mu\text{m}$   
57 were  $0.04 \pm 0.02 \text{ cm}^{-3}$  ( $0.1 \text{ cm}^{-3}$  highest,  $0.02 \text{ cm}^{-3}$  lowest), typical for the warm season in this  
58 region and representing  $\sim 9\%$  of all particles in this size range as a campaign average.

59           The primary focus of FIN-03 was the measurement of INP concentration via immersion  
60 freezing at temperatures  $> -33 \text{ }^\circ\text{C}$ . Additionally, some measurements were made in the  
61 deposition nucleation regime at these same temperatures, representing one of the first efforts to  
62 include both mechanisms within a field campaign. INP concentrations via immersion freezing  
63 reported by all ice nucleation instruments generally agreed to within one order of magnitude for  
64 measurement and sampling times coordinated to within three hours. Sometimes, much better  
65 agreement was obtained. Outliers of up to two orders of magnitude occurred between  $-25 \text{ }^\circ\text{C}$  and  
66  $-18 \text{ }^\circ\text{C}$ ; better agreement was seen at higher and lower temperatures. INP activity in the



67 immersion freezing mode was generally found to be an order of magnitude or more efficient than  
68 in the deposition regime at 95-99% water relative humidity, although this limited data set should  
69 be augmented in future efforts.

70 To contextualize the study results an assessment was made of the composition of INPs  
71 during the late Summer to early Fall period of this study, inferred through comparison to existing  
72 ice nucleation parameterizations and through measurement of the influence of thermal and  
73 organic carbon digestion treatments on immersion freezing ice nucleation activity. Consistent  
74 with other studies in continental regions, biological INPs dominated at temperatures  $> -20$  °C  
75 and sometimes colder, while arable dust-like or other organic-influenced INPs were inferred to  
76 dominate at most times below  $-20$  °C.



77 **1 Introduction**

78 Atmospheric ice nucleation is one of the least certain aerosol-cloud interactions  
79 influencing climate (Kanji et al., 2017). Aerosols that physically catalyze freezing, known as ice-  
80 nucleating particles (INPs) (Vali et al., 2015), are found in the atmosphere in concentrations that  
81 span many orders of magnitude, ranging from  $10^{-3} \text{ L}^{-1}$  or fewer at  $-5 \text{ }^{\circ}\text{C}$  to  $1000 \text{ L}^{-1}$  or greater at  
82  $-35 \text{ }^{\circ}\text{C}$  (Petters and Wright, 2015). INP number concentrations typically increase exponentially  
83 with degree of supercooling below  $0 \text{ }^{\circ}\text{C}$ . However, chemical composition plays an important role  
84 in determining if, and at what temperature, individual particles may serve as INPs (Murray et al.,  
85 2012). INPs initiate the formation of ice in cold and mixed-phase clouds and in turn influence  
86 their physical and optical properties. An increase in INP concentration over a geographic area  
87 may increase the frequency of glaciated clouds at constant temperature, which in turn increases  
88 precipitation and decreases cloud lifetime (Lohmann and Feichter, 2005). Nevertheless, INP  
89 impacts on clouds simulated in global climate models are highly sensitive to how aerosol's  
90 ability to nucleate ice is parameterized (Boucher et al., 2013). Parameterizations can only be as  
91 accurate as the measurements on which they are based (e.g., Knopf et al., 2021).

92 Measurements of atmospheric INPs remain challenging due to the difficulty representing  
93 the physical processes involved in ice nucleation instruments. At temperatures below  $\sim -38 \text{ }^{\circ}\text{C}$ ,  
94 micrometer-sized, dilute water droplets spontaneously freeze due to homogeneous freezing  
95 nucleation. Homogeneous freezing nucleation is well understood and included in most cloud  
96 formation models. However, at temperatures between  $0$  and  $-38 \text{ }^{\circ}\text{C}$ , freezing requires INPs to  
97 facilitate nucleation through a heterogeneous nucleation mechanism (Kanji et al., 2017; Murray  
98 et al., 2012; Vali, 1985). Nucleation is hypothesized to proceed through (1) immersion freezing,  
99 which occurs when an INP embedded within a water droplet enters a cooler environment, and  
100 nucleates an ice crystal, (2) condensation freezing, which occurs when freezing ensues as an



101 aqueous droplet condenses on the surface of an aerosol particle, (3) contact freezing, which  
102 occurs when an aerosol in contact with a water droplet surface initiates freezing (Durant and  
103 Shaw, 2005; Fornea et al., 2009), and (4) deposition nucleation, which is thought to occur  
104 through the direct deposition of water vapor on an INP surface. Of these mechanisms,  
105 immersion freezing nucleation is thought to be the most active heterogeneous nucleation process  
106 in the atmosphere, though there is considerable disagreement in the literature about the relative  
107 importance of other mechanisms (Kanji et al., 2017; Ullrich et al., 2017). When the ambient  
108 humidity is below water saturation, nucleation can occur via deposition of water from the vapor  
109 phase. In some cases, this behavior may be ascribable instead to water condensation in pores and  
110 cavities in aerosols facilitating freezing through a non-deposition mechanism (Marcolli, 2014;  
111 Wagner et al., 2016). However, this process is unlikely to be of importance at temperatures  $> -38$   
112  $^{\circ}\text{C}$  (David et al., 2020), which are the focus of this study. We will thus refer to ice nucleation at  
113  $> -38$   $^{\circ}\text{C}$  and below water saturation as happening within the “deposition regime”. Study of the  
114 efficiency of the deposition nucleation process in comparison to immersion freezing has been  
115 limited for natural INPs.

116 Ice nucleation measurements have been made with instruments designed and built by  
117 individual scientists, and more recently with commercial instruments. The ice nucleation  
118 community has a history of collaborating to address instrument performance and inconsistencies  
119 through participating in instrument intercomparisons, in which the custom-built instruments were  
120 operated side-by-side, to evaluate instrument response to the same aerosol populations (Coluzza  
121 et al., 2017; DeMott et al., 2011, DeMott et. al, 2018; Knopf et al, 2021; Lacher et al., 2024). To  
122 compare concentrations and compositions of INPs, a three-part workshop series, the Fifth  
123 International Ice Nucleation Workshop, or “FIN” was held in 2014-2015. The first two phases



124 were held at the Karlsruhe Institute of Technology’s Aerosol Interactions and Dynamics in the  
125 Atmosphere (AIDA) facility. FIN-01 focused on determination of composition of INPs by mass  
126 spectroscopy (Shen et al., 2024, in preparation), while FIN-02 entailed a laboratory ice nucleation  
127 instrument comparison (DeMott et al., 2018). FIN-03, the mountaintop field intercomparison of  
128 ice nucleation instruments is the focus of this manuscript.

129 Ice nucleation measurements have experienced a renaissance in the past decade, resulting  
130 in a proliferation in both the number of custom-built instruments and a diversification of  
131 measurement techniques employed (Zenker, 2017; DeMott, 2018; Möhler, 2021). Participation in  
132 FIN-02 was twice that of the previous formal international workshop intercomparison in 2007 (the  
133 International Workshop on Comparing Ice Nucleation Measuring Systems, or ICS-2007 held at  
134 the (AIDA) facility (Jones et al., 2011; Kanji et al., 2011). During FIN-02, online and offline  
135 instruments sampling the same population of aerosolized particles reported INP concentrations  
136 that generally agreed within one order of magnitude across a broad temperature range. Agreement  
137 was best in tests of immersion freezing on soils, dusts and bacteria but spanned up to 2 orders of  
138 magnitude (or 3 °C in temperature for the same active site density) for illite NX and K-feldspar  
139 (DeMott et al., 2018). While relatively good agreement in the laboratory between different  
140 measurement methods during FIN-02 represents significant progress for the atmospheric ice  
141 nucleation community, intercomparisons in ambient atmospheric settings are more difficult due to  
142 lower typical INP concentrations (Lacher et al., 2018) and variations in the chemistry and size of  
143 source aerosol and INPs (DeMott et al., 2017; Knopf, 2021; Lacher et al., 2024).

144 To evaluate how a suite of instruments operating collectively perform under the greater  
145 measurement challenges of the field setting, FIN-03 was conducted from September 12 to 28, 2015  
146 at Storm Peak Laboratory (SPL) in Steamboat Springs, CO, USA (Elevation: 3220 m MSL).



147 Unlike the subsequent closure studies of Knopf et al. (2021) and the similar comparative sampling  
148 studies of Lacher et al. (2024), both of which occurred in regions surrounded by agricultural  
149 activities and possible nearby urban influences, this remote continental mountaintop site at an  
150 elevation of 3220 m provided the opportunity to sample both regional and long-range INP sources  
151 within both the boundary layer and free troposphere. The site is typically in the free troposphere  
152 during the nighttime and early morning, and in the boundary layer from the late morning to early  
153 evening, although topography and wind direction influence this timing (Collaud Coen et al., 2018).  
154 When in the free troposphere, the site is more likely to reflect influences by regional or long-range  
155 transport of aerosols. For example, during FIN-03, the variety of air masses that were sampled and  
156 sensed by aerosol instruments included ones passing over phosphate mines in Idaho (on September  
157 18 and 20) and mined deposits of rare earth metals at Mountain Pass, CA (on September 27)  
158 (Zawadowicz et al., 2017). When the convective boundary layer height reaches the elevation of  
159 the laboratory, the site is likely more impacted by local/regional aerosol sources. Additionally,  
160 meteorological transitions can occur (e.g., frontal boundary passage, wind direction shifts), driving  
161 changes in aerosol sources that may indirectly occur in response to those changes (e.g., biological  
162 aerosols, carbonaceous particles from biomass burning, and mineral/soil dust). While the  
163 constantly fluctuating environmental conditions during FIN-03 added an additional challenge to  
164 the intercomparison, they also provided a realistic setting for atmospheric INP measurements. In  
165 addition to adding challenges, conducting the intercomparison in the presence of complex aerosols  
166 in the field provided the opportunity to survey instrument response to varied aerosol sources.

167 Participation in FIN-03 included online continuous flow diffusion chambers (CFDCs) and  
168 aerosol collections for offline INP measurements, representing a subset of the instruments that  
169 operated in FIN-02 (DeMott et al., 2018). Since aerosol physical and chemical properties strongly



170 influence their ability to activate as INPs (Hoose and Möhler, 2012; Kanji et al., 2017; Murray et  
171 al., 2012), measurements of aerosol sizes and composition (see Section 2) were included to lend  
172 context to the variable composition of aerosols and evaluate their potential role in ice nucleation  
173 activity. Rather than use these data for attempting closure, FIN-03 focused on using data to  
174 constrain existing parameterizations to diagnose INP compositions during the study period. Also,  
175 in contrast to other recent studies, special effort was made to characterize deposition nucleation  
176 activity in addition to immersion freezing.

## 177 **2 Methods**

### 178 **2.1 Aerosol property measurements**

179 Measurements of aerosol physical, chemical, and biological particle properties were  
180 made during FIN-03 to provide context to INP measurements. Sampling manifolds, which draw  
181 air into SPL from outdoors at high flow, are as follows: Inlets were located in each of the two  
182 wings of SPL that frame the living area, referred to as the “instrument” laboratory (facing north)  
183 and the “chemistry” laboratory (facing south). The “original” inlet system in the instrument  
184 laboratory (Hallar et al. 2011; Petersen et al. 2019) feeds a nephelometer (see below) and a  
185 standard suite of aerosol instruments (not operational for FIN-03). This 15 cm diameter  
186 aluminum inlet rises 4 m above the roofline. At ~1 m inside the laboratory, it transitions to a 15  
187 cm horizontal manifold. With a flow of ~500 L min<sup>-1</sup>, aerosol transmission calculations have  
188 characterized the system to have a 50% upper particle size cut-off at an aerodynamic diameter of  
189 5 μm (Hallar et al., 2011). The “new” inlet system consists of two identical stainless steel,  
190 turbulent-flow, ground-based inlets described by Petersen et al. (2019), which are straight and  
191 enter the laboratory vertically. One is in the SPL instrument laboratory, and one is in the  
192 chemistry laboratory. These inlets that extend 10 m above the laboratory roof have been





193 demonstrated to have 50% upper particle size cut-offs at an aerodynamic diameter of  
194 approximately  $13\mu\text{m}$  for a wind speed of  $0.5\text{ m s}^{-1}$ . Additional computational fluid dynamics  
195 simulations suggest that this size cut off remains above  $5\mu\text{m}$  even for exterior wind speeds up to  
196  $15\text{ m s}^{-1}$  (Petersen et al., 2019), higher than achieved at any time during FIN-03 sampling. Little  
197 bias was seen in ambient aerosol sampling between the original inlet system and the new,  
198 turbulent flow-based inlets based on the metric of total aerosol scattering (Petersen et al., 2019).  
199 Flow rates and transfer lines to individual instruments are described after the aerosol property  
200 measurements are introduced, at the conclusion of this section.

201           A Laser Aerosol Spectrometer (LAS, model 3340, TSI Inc., St. Paul, Minnesota, USA)  
202 was used to measure the aerosol size distribution over the diameter range  $0.089\text{-}10\mu\text{m}$ . Aerosols  
203 were assumed dry based on relative humidity always remaining below 30% when measured from  
204 its sample line. Sample was drawn at  $0.1\text{ L min}^{-1}$  and sampling was done from the turbulent flow  
205 inlet system located in the SPL chemistry laboratory, as described further below. Size  
206 calibrations were performed using polystyrene latex spheres (PSL, Duke Scientific). PSL  
207 diameters were converted to ammonium sulfate equivalent diameters using Mie theory (Froyd et  
208 al., 2019). Particle concentrations are reported as a function of equivalent ammonium sulfate  
209 diameter. Volume and surface area distributions are derived assuming spherical particles.  
210 Number concentrations and surface areas, further informed by aerosol composition  
211 measurements, allows for connection to INP concentration predictions, and this information is  
212 used herein to diagnostically infer mineral and soil dust influences on INPs during the study. We  
213 will particularly reference the parameterizations of Niemand et al. (2012) that links mineral  
214 surface area to INP concentrations and DeMott et al. (2015) that links dust number  
215 concentrations at sizes larger than  $0.5\mu\text{m}$  to INP concentrations.



216 Measurements using a three-wavelength integrating nephelometer (TSI Model-3563,  
217 Shoreview, MN) also provided information on aerosol distributions via their optical properties.  
218 This nephelometer is part of the National Oceanic and Atmospheric Administration Federated  
219 Aerosol Network (Andrews et al., 2019). The nephelometer splits scattered light into red (700  
220 nm), green (550 nm), and blue (450 nm) wavelengths. Impactors to cut aerosols at aerodynamic  
221 sizes below 1 and 10  $\mu\text{m}$  are alternately used upstream of air flowing into the instrument. The  
222 nephelometer sampled within the original inlet in the SPL instrument laboratory. A blunt tap  
223 from this original SPL inlet manifold provided air samples to the nephelometer system via 1" i.d.  
224 conductive tubing.

225 The Particle Analysis by Laser Mass Spectrometry (PALMS) instrument performed  
226 measurements of the composition of 0.2 to 3.0  $\mu\text{m}$  aerosol particles. The PALMS was designed  
227 and operated by the National Oceanic and Atmospheric Administration (NOAA) as described in  
228 Thomson et al. (2000). Particles are sampled, focused, and accelerated via an aerodynamic lens  
229 inlet (Schreiner et al., 2002) before passing into a vacuum chamber where they successively pass  
230 through two continuous-wave detection laser beams (532 nm Nd:YAG) and scatter light.  
231 Vacuum aerodynamic diameter is determined based on the transit time. The detection signal  
232 triggers an ArF excimer laser that emits a 193 nm pulse to simultaneously ablate and ionize  
233 single particles. The resulting ions are analyzed with a unipolar time-of-flight mass spectrometer,  
234 which allows polarity switching during the particle flight and thereby producing positive or  
235 negative mass spectra for individual particles. PALMS spectra are classified into compositional  
236 categories, and fractions are averaged over 5 min sample periods. Number, surface area, and  
237 mass concentration products for the different particle types are generated by combining PALMS  
238 size-dependent fractional composition data with absolute particle concentrations measured by the



239 LAS instrument (Froyd, et al. 2019; Froyd et al., 2022). When PALMS compositional  
240 concentrations are referenced in the results of FIN-03 aerosol compositions in Section 3.2, they  
241 have been determined by these methods.

242 The NOAA Wideband Integrated Bioaerosol Sensor, Model 4A (WIBS-4A; Droplet  
243 Measurement Technologies, Longmont, CO) was used to detect fluorescent properties of  
244 individual particles and assess the presence of biological particles. Measurements are presumed  
245 to characterize dry particles. The WIBS-4A is described in detail elsewhere (Gabey et al., 2010;  
246 Kaye et al., 2005; Perring et al., 2015) and is only briefly summarized here. As described in  
247 Zawadowicz et al. (2019), the gain for the WIBS-4A used at SPL was set to detect and classify  
248 particles between 0.4 and 10  $\mu\text{m}$ . First, the optical diameter of particles entering the detection  
249 cavity is determined by light scattered during transit through a 635 nm laser beam. This signal  
250 triggers the sequential firing of two xenon flash lamps filtered to produce narrow excitation  
251 wavebands centered at 280 and 370 nm. The resulting fluorescence is detected by two wideband  
252 photomultiplier detectors observing 310-400 nm and 420-650 nm. Fluorescing particles were  
253 categorized according to the intensity of the signal in each of three channels (channel A  
254 excitation 280 nm/emission 310-400 nm, channel B excitation 280 nm/emission 420-650 nm,  
255 channel C excitation 370 nm/emission 420-650 nm). Particles for which the measured emission  
256 intensity in only one channel met the threshold (such that the signal intensity exceeded the value  
257 equal to three standard deviations above the mean) were assigned Type A, B, or C, and particles  
258 for which the measured emission intensity in two or more channels met the threshold were  
259 assigned Type AB, BC, BC, or ABC (Perring et al., 2015). The interpretation of particle  
260 composition according to the seven WIBS-4A channels is not straightforward, as many  
261 fluorophores are active in each channel, including non-biological components (Perring et al.,



262 2015; Pöhlker et al., 2012). Channel A fluorophores include biological components such as  
263 tryptophan, phenylalanine as well as nonbiological components which interfere with the  
264 determination of biological content, including polycyclic aromatic hydrocarbons (PAHs)  
265 (pyrene, naphthalene, phenanthrene). Biological fluorophores, which produce a signal in channel  
266 C, include the reduced form of nicotinamide adenine dinucleotide (NADH), nicotinamide  
267 adenine dinucleotide phosphate (NADPH), and riboflavin, and potential non-biological  
268 interference in channel C may result from the presence of humic acid in aerosol particles.  
269 Channel B fluorophores are not generally considered to be biological in nature, though riboflavin  
270 and dry cellulose both produce signals in this channel.

271 We report WBS-4A channel data herein under these noted caveats and further utilize  
272 these data to explore links to immersion freezing biological INP concentrations, as has been done  
273 in some previous efforts. Tobo (2013) previously reported relations of biological INPs acting in  
274 the immersion freezing mode (measured by the CSU CFDC) to fluorescent biological aerosol  
275 particles (FBAP) at sizes  $> 0.5 \mu\text{m}$  measured in the understory of a Ponderosa pine forest in  
276 Colorado. In that work, an ultraviolet aerodynamic particle sizer (UV-APS) with excitation  
277 wavelength at 355 nm and emission wavelengths 420-575 nm was used as a reference for FBAP  
278 concentrations. Due to differences between the excitation and emission wavelengths, UV-APS  
279 measurements correspond most closely with Type C particles detected by the WBS-4A (Healy  
280 et al., 2014). Consequently, a conservative or “low” estimate of FBAP for use in the  
281 parameterization of Tobo et al. (2013) we employ herein uses the sum of C, AC, BC and ABC  
282 particles. A “high” FBAP for this parameterization has also been used by Twohy et al. (2016),  
283 considering all non-B-only particles (A, AB, ABC, AC, BC, C). We will use both definitions in  
284 our presented results and partly justify the higher estimate because the CSU CFDC assuredly



285 does not capture all biological INPs due to the use of the upstream impactor. A final class of  
286 particles defined by WIBS-4A data for relation to immersion freezing INPs are denoted as FP3  
287 particles (Wright et al., 2014). FP3 particles are particles that show strong emission in the 310 to  
288 400 nm spectral band when excited by 280 nm light (A type) but are only weakly represented as  
289 B and C types. A threshold of 1900 arbitrary fluorescence units in the 310 to 400 nm band is  
290 used to denote FP3 particles (Wright et al., 2014). FP3 particles have been connected to  
291 immersion freezing INP concentrations in multiple environments (Wright et al., 2014; Suski et  
292 al., 2018; Cornwell et al., 2023).

293 Flow rates and transfer lines to each instrument are summarized as follows. The PALMS,  
294 LAS, and WIBS-4A sampled from the SPL turbulent flow inlet stack at 0.75, 0.1, and 0.3 vlp<sub>m</sub>,  
295 respectively, via a common 1/4" o.d. aluminum tube. The total flow was held at 1.2 vlp<sub>m</sub> using  
296 a variable dump flow, and the line was split into multiple 1/8" o.d. stainless steel tubing sections  
297 connecting to each instrument. All tubing junctions employed Y-splitters, and all reducing  
298 fittings were internally beveled to prevent impaction losses. Sample lines were not actively dried,  
299 but relative humidity was < 30% in LAS and WIBS-4A. For the LAS instrument, the theoretical  
300 transmission of the inlet system was 98%, 84%, and 57% for 1, 3, and 5 μm aerodynamic  
301 diameter particles, respectively, with gravitational settling being the dominant loss process.  
302 Transmission to WIBS-4A for the same sizes was 99%, 90%, and 76%. Size distributions were  
303 not corrected for transmission losses. The nephelometer sampled from the original inlet in the  
304 SPL instrument laboratory via a blunt tap manifold and 1" i.d. conductive tubing.

305

306

307

308



309 **Table 1** Descriptions of INP instruments.

	Instrument	Type	Institute	References
Online/direct	Continuous flow diffusion chamber (CSU-CFDC)	Continuous flow diffusion chamber (cylindrical)	Colorado State University	(Eidhammer et al., 2010; Rogers, 1988; Rogers et al., 2001)
	Spectrometer for ice nuclei (MIT-SPIN)	Continuous flow diffusion chamber (parallel)	Massachusetts Institute of Technology	(Garimella et al., 2016; Garimella et al., 2017; Kulkarni & Kok, 2012)
Offline/post-processing	Frankfurt Ice Nuclei Deposition Freezing Experiment deposition mode (FRIDGE-DEP)	Low pressure diffusion chamber (on wafers)	Goethe University Frankfurt	(Schrod et al., 2016)
	Frankfurt Ice Nuclei Deposition Freezing Experiment immersion freezing mode (FRIDGE-IMM)	Cold stage droplet freezing array (on wafers)	Goethe University Frankfurt	(Schrod et al. 2020; DeMott et al. 2018)
	Ice spectrometer (CSU-IS)	Aliquot freezing array	Colorado State University	(Hill et al., 2016; Hiranuma et al., 2015)
	Cold stage (NC State-CS)	Cold stage droplet freezing array (on hydrophobic glass slides)	North Carolina State University	(Wright & Petters, 2013; Yadav et al., 2019)

310

311 **2.2 INP measurement methods**

312 A combination of direct-processing (online) and post-processing (offline) ice nucleation  
 313 instruments were employed during the FIN-03 field campaign. All these instruments were also  
 314 used in the FIN-02 laboratory campaign. Online instruments have the advantage in that the  
 315 aerosol being evaluated as INPs remain free-floating and unaltered, never touching a substrate  
 316 nor requiring shipment of samples to a laboratory. Online techniques can also monitor INP



317 concentration changes occurring over short time scales. Nevertheless, they are limited in the  
318 thermodynamic conditions that can be represented over a given time frame, and they are limited  
319 by volume sampling rates in assessing the low concentrations of INPs at modest supercooling.  
320 Offline techniques, i.e., those in which samples are collected in the field and subsequently  
321 processed in laboratory, provide the opportunity to capture large sample volumes (albeit over  
322 longer time scales) and consequently assess a wider temperature range of INP activation  
323 properties. A summary listing of all ice nucleation instruments is provided in Table 1. Detailed  
324 operating principles, siting of samplers (rooftop versus within SPL), and experimental methods  
325 for each instrument follow below. In this work, we will refer to the FIN-03 “intercomparison  
326 period” to define the times that all INP instruments co-sampled air with substantial temporal  
327 overlap for direct comparison. Other times of sampling by the different instrument groups were  
328 devoted to special science investigations that are not covered herein.

329

### 330 ***2.2.1 Online INP measurements***

331 Two online instruments participated in intercomparison experiments in FIN-03. One, the  
332 Colorado State University CFDC (CSU-CFDC), has the most established history as an online  
333 technique for activating and counting INPs. The CSU-CFDC operating principles are described  
334 in several prior works (Rogers, 1988; Rogers et al., 2001; Eidhammer et al., 2010). Application  
335 and considerations for interpreting data have been described in detail in several publications,  
336 most recently by DeMott et al. (2018). The CSU-CFDC is composed of nested cylindrical copper  
337 walls that are chemically ebonized to be hydrophilic so they can be evenly coated with ice. The  
338 chamber is divided into two sections vertically. For FIN-03, the CSU-CFDC was operated to  
339 establish a temperature gradient between the colder (inner) and warmer (outer) ice walls in the



340 upper ~50 cm “growth” section to produce either water subsaturated or water supersaturated  
341 conditions at various temperatures within a central lamina. For the flow rates used (10 vlp total  
342 flow, 1.5 vlp sample flow) the residence time was ~5 s in the growth region. Aerosol particles  
343 were directed into that central lamina. Ice crystals forming on INPs in the growth section  
344 continued to grow for ~2 s in the lower ~35 cm “evaporation” section of the chamber where the  
345 outer wall temperature was adjusted to be at an equivalent temperature to the inner (cold) wall to  
346 promote evaporation of liquid drops. When operating in the water supersaturated regime, water  
347 relative humidity was controlled to be nominally at 105% during FIN-03 to stimulate droplet  
348 growth and subsequent freezing, for best comparison to offline immersion freezing methods. For  
349 probing ice nucleation in the deposition nucleation regime, relative humidity (RH) was  
350 controlled to ~95%.

351 The CSU-CFDC sampled from one of the turbulent aerosol inlet ports, located in the SPL  
352 instrument laboratory. Connection was via ¼” o.d. conductive tubing. Prior to entering the CFDC,  
353 aerosol was further dried using two inline diffusion driers and then size-limited using dual single-  
354 jet impactors that achieve a 50% upper particle size cut-off at an aerodynamic diameter of 2.5 µm.  
355 This limitation on aerosol sizes helps to remove ambiguity when distinguishing ice crystals at ~4  
356 µm sizes from aerosol particles using an optical particle counter at the CSU-CFDC outlet.  
357 Temperature uncertainty is ± 0.5 °C at the reported CSU-CFDC lamina processing temperature  
358 and relative humidity uncertainty depends inversely on temperature, as discussed by DeMott et al.,  
359 (2018), estimated for example as 2.4 % at –25 °C.

360 To correct for background counts that can occur due to ejection of frost emanating from  
361 interior surfaces of the CSU-CFDC over operational periods, and for defining measurement  
362 uncertainties, we follow Levin et al. (2019). Frost corrections are defined through intervals of





363 sampling ambient air through a HEPA filter. Sample data were background corrected by  
364 subtracting the interpolated filter period concentration before and after each sampling period.  
365 Background corrected data were then averaged to ~5-min sampling times to increase statistical  
366 confidence. Poisson counting errors during filtered and ambient sampling periods were added in  
367 quadrature, and INP concentrations were judged statistically significant at the 95% confidence  
368 level if they were greater than 1.64 times this combined INP error (one-tailed z test). Interior inlet  
369 tubing losses are not considered in the reported INP data because they have been estimated at 10%  
370 or less in the past. INP concentration correction underestimates inferred (by 3 time) to be due to  
371 aerosols spreading outside of the lamina during measurements specifically of mineral dust INPs  
372 (DeMott et al., 2015) are not generally applied to the data herein, though this is discussed regarding  
373 INP parameterizations in this paper.

374 An aerosol concentrator (MSP Model 4240) was used at selected times during FIN-03 to  
375 improve sampling statistics, in the same manner as in previously published studies (Tobo et al.  
376 2013; Suski et al., 2018; Cornwell et al., 2019). The aerosol concentrator was positioned open to  
377 the air on the roof of the instrument laboratory room (covered and not used during rainfall), with  
378 a short ¼" o.d. copper line containing the concentrated aerosol entering the laboratory from about  
379 3 m above the CFDC. Concentration factors were evaluated in the same manner as Tobo et al.  
380 (2013), leading to an average increase of INPs by 90 times during operation of the aerosol  
381 concentrator compared to ambient inlet periods during the study (not shown here because analysis  
382 repeats numerous past efforts).

383 A three-way manual stainless-steel valve was used to direct sample air to the CFDC from  
384 either the turbulent flow inlet or the aerosol concentrator. At times, a high temperature heating  
385 tube (Suski et al., 2018) or a single particle soot photometer (Schill et al., 2016) was placed in-line



386 following the three-way valve for removing aerosol organics or black carbon (not reported here)  
387 prior to INP measurements. The use of a tube heater upstream of the CSU CFDC to expose single  
388 particles to 300°C, following the methods of Suski et al. (2018), is intended to isolate the action  
389 of total organic versus inorganic INPs via comparison of ambient versus heat-treated particle  
390 streams. Simultaneous measurements of both aerosol streams is of course not possible with a single  
391 CFDC, so sampling was conducted by alternating the inlet chosen during subsequent 10-minute  
392 periods, and ignoring any very short-term aerosol changes that might occur over such times. This  
393 was a special contribution by the CSU CFDC group, for comparison to bulk aerosol treatments  
394 discussed in the next subsection.

395         A second online instrument, the SPectrometer for Ice Nuclei operated at the time by the  
396 Massachusetts Institute of Technology (MIT-SPIN; Droplet Measurement Technologies, Boulder,  
397 CO), a commercially produced, parallel-plate continuous flow diffusion chamber style instrument,  
398 also sampled during FIN-03. Operating principles are described in Garimella et al. (2016) and  
399 Garimella et al. (2017). SPIN consists of two flat walls separated by 1.0 cm and coated in  
400 approximately 1.0 mm of ice. Aerosol particles are fed into the chamber in a lamina flow of about  
401 1.0 liters per minute and are constrained to the centerline with a sheath flow of about 9.0 liters per  
402 minute. The temperature and relative humidity that the aerosol lamina experiences are controlled  
403 by varying the temperature gradient between the two iced walls (Kulkarni & Kok, 2012). After  
404 exiting the nucleation chamber, the particles enter SPIN's optical particle counter, which sizes  
405 aerosol on a particle-by-particle basis for diameters between 0.2 and 15  $\mu\text{m}$ . For FIN-03, the SPIN  
406 sampled from one of the turbulent flow inlet systems, located within the SPL aerosol chemistry  
407 laboratory. It was connected to the inlet system port with a short section of ¼" o.d. conductive  
408 tubing.



409 Data processing for SPIN was performed following a similar procedure as the CSU-CFDC  
410 instrument. Particle counts from the OPC were first filtered to only consider particles larger than  
411  $5 \mu\text{m}$ . A low-pass filter was applied next to remove all 1 Hz data that exceeded a total of three  
412 counts. Particle data was then converted from counts per second to number density ( $\text{n L}^{-1}$ ) using  
413 the combined sheath and sample flow exiting the OPC. A SPIN specific particle concentration  
414 correction factor of 1.4 is applied to account for non-ideal instrument behavior resulting in  
415 underestimation of INP as described by Garimella et al. (2017). As the field measurements from  
416 this study predate the laboratory experiments performed to determine SPIN uncertainties, we select  
417 the minimum reported correction factor to remain conservative in our measurements. A  
418 depolarization filter was then applied to isolate particle data specific to ice using 1 Hz averaged  
419 backscattering data from the SPIN's OPC, with instrument specific values of 3.5 and -0.25 for the  
420  $\log_{10}(\text{Size})$  and  $\log_{10}(\text{S1/P1})$  measurements respectively. Frost ejected from the plates of the SPIN  
421 chamber was characterized by particle-free sampling periods when the sample flow was diverted  
422 through a HEPA filter by an automated three-way valve. Linear interpolation was used to  
423 approximate background frost throughout the measurement period and smoothed using a five-  
424 minute moving average. Sample data was background frost corrected by subtracting this smoothed  
425 background frost density from total number density. Lastly, data points that exceeded water  
426 saturation were excluded from analysis.

427 Estimation of measurement error for the MIT-SPIN follows a similar procedure to the  
428 CSU-CFDC. Assuming the background corrected INP concentration follows a Poisson  
429 distribution, the Poisson error for both INP and background frost concentrations were defined as  
430 the square root of the sample mean. The significance test statistic was defined by the quadrature  
431 sum of counting errors multiplied by the z-score for a one-tailed z-test at the 95% confidence



432 interval. INP measurements were deemed statistically significant if the mean INP concentration  
433 was greater than this test statistic.

434 A third online instrument, the Texas A&M CFDC that shares the same design aspects of  
435 the CSU CFDC, was used for special studies conducted outside of intercomparison exercises  
436 (Zenker et al., 2017).

### 437 ***2.2.2 Offline INP measurements***

438 Offline methods have undergone many improvements in recent years and have been  
439 successfully demonstrated for being used in a complementary manner to online methods in other  
440 recent intercomparisons (DeMott et al., 2017; DeMott et al., 2018; Hiranuma et al., 2015; Wex et  
441 al., 2015). In FIN-03 samples were collected with liquid impingers and filter samplers and  
442 analyzed for immersion freezing of distributed liquid particle suspensions using the North  
443 Carolina State University Cold Stage (Wright et al., 2013), the CSU Ice Spectrometer (Hiranuma  
444 et al., 2015; DeMott et al., 2018), and the FRankfurt Ice Nuclei Deposition FreezinG Experiment  
445 (FRIDGE) instrument (Schrod et al., 2016).

#### 446 The North Carolina State University Cold Stage (NC State-CS)

447 The North Carolina State University cold stage (NC State-CS), previously described by  
448 Wright and Petters (2013) and Hader et al. (2014). Procedures used for collecting immersion  
449 freezing spectra are described below and by Yadav et al. (2019). During FIN-03, filter samples,  
450 impinger samples and precipitation samples were collected for analysis using the NC State-CS.  
451 For the intercomparison, the filter and impinger results are considered. Filter samples were  
452 collected from the roof of Storm Peak Lab for 3–4 hrs twice daily using 47 mm Nuclepore  
453 polycarbonate filters (0.2  $\mu\text{m}$  pore size) housed in an open-faced stainless-steel filter holder  
454 operated at 14 L  $\text{min}^{-1}$  (at altitude) or  $\sim 9$  L  $\text{min}^{-1}$  at standard temperature and pressure conditions



455 (STP) of 1013 mb and 0 °C. Filter holders were directed downward and sheltered from  
456 precipitation by a large, inverted metal bowl. Images are shown in supplemental Section S1.  
457 Impinger samples were collected directly into water using a glass bioaerosol impinger (SKC, Inc.)  
458 as described by Hader et al. (2014) and DeMott et al. (2018). The impinger jets air at 10.6 L min<sup>-1</sup>  
459 (~7 L min<sup>-1</sup> STP) into a 20 mL water reservoir, impacting 80% of particles ≥ 200 nm in diameter  
460 and ~100% of particles ≥ 1 μm (Willeke et al., 1998). Impinger samples were collected in the same  
461 manner as was done for all shared liquid samples for the FIN-02 intercomparison (DeMott et al.,  
462 2018) excepting that Teflon tape replaced stopcock grease to seal the impinger glass lid to prevent  
463 jamming. Water evaporating from the reservoir was replaced hourly; the impinger was in a rooftop  
464 shelter with its inlet extending through a hole in the shelter wall, into the open air at a height of ~6  
465 feet below the position of filter sampling units that were mounted on an outside railing. Water used  
466 onsite was filtered (0.2 μm) Milli-Q water. All samples were stored at -20 °C onsite, shipped on  
467 dry ice, then stored at -80 °C until analysis.

468 Freezing statistics for each liquid sample were acquired by pipetting an array of  
469 approximately 256 droplets of 1 μL ± 0.88% volume on four hydrophobic glass slides under dry  
470 N<sub>2</sub> gas. Temperature was ramped at a rate of -2 °C min<sup>-1</sup> and freezing was detected optically by a  
471 microscope at a temperature resolution of 0.17 °C (every 5 s). Freezing temperature spectra are  
472 expected to be independent of cooling rate (Wright et al., 2013). The concentration of ice nuclei  
473 at temperature  $T$  per unit volume of liquid is given by Vali (1971):

$$474 \quad c_{IN}(T) = \frac{-\ln(f_{unfrozen}(T))}{V_{drop}\Delta T} \quad (1)$$

475 where  $f_{unfrozen}$  is the fraction of unfrozen droplets at  $T$  and  $V_{drop}$  is the population-median droplet  
476 volume. The concentration of ice nucleating particles (INP) in the atmosphere is given by:



477 
$$c_{INP}(T) = \frac{c_{IN(T)} \cdot f \cdot V_{liquid}}{V_{air}} \quad (2)$$

478 where  $f$  accounts for sample dilution,  $V_{liquid}$  is sample volume, and  $V_{air}$  is the volume of air  
479 sampled (flow rate at STP  $\times$  duration). Freezing spectra were collected 3 $\times$  per sample and binned  
480 into 1 °C intervals. Confidence intervals reported in archived data are  $\pm 2$  standard deviations of  
481 the mean. We will refer to the processed filter samples as NC State-CS (F) and processed  
482 impinger samples as NC State-CS (I).

483 CSU Ice Spectrometer (CSU-IS)

484 The CSU-IS also post-processed particles sampled onto filters during FIN-03. This  
485 instrument has been described in Hiranuma et al. (2015) and Suski et al. (2018). Samples were  
486 collected for approximate periods of 4 hours for intercomparison periods (longer for overnight  
487 samples – not part of the intercomparison) using pre-cleaned 0.2  $\mu\text{m}$  pore diameter, 47 mm  
488 polycarbonate Nuclepore filters (Suski et al., 2018) mounted in disposable, sterile open-faced and  
489 face-up holders (Nalgene), with a typical sample flow rate of 14.9 L  $\text{min}^{-1}$  (ambient) and 9.5 L  
490  $\text{min}^{-1}$  (STP). Filters were collected on the same exterior laboratory roof railing as the NC State  
491 filters, approximately 2 m distance away. All filter samples were frozen following collection, and  
492 until processing at CSU. Pre-sterilization procedures and overall clean protocols for preparation  
493 and handling of filters are detailed in Suski et al. (2018). Particle re-suspension was done through  
494 20 minutes of shaking filters in sterile 50 mL Falcon polypropylene tubes (Corning Life Sciences)  
495 with 6-10 mL of 0.02  $\mu\text{m}$  pore diameter filtered deionized water. Further 20-fold dilutions using  
496 filtered water were made as needed to permit measurement of freezing spectra to the low  
497 temperature limit of operation of the CSU-IS.

498 Immersion freezing INP temperature spectra were obtained by distributing 24 - 32 aliquots  
499 of 50  $\mu\text{L}$  particle suspensions into the sterile 96-well PCR trays that mount in the CSU-IS. The



500 cooling rate was  $-0.33\text{ }^{\circ}\text{C min}^{-1}$ . Frozen wells were counted at  $0.2 - 1\text{ }^{\circ}\text{C}$  degree intervals to a limit  
501 of about  $-28\text{ }^{\circ}\text{C}$ , and cumulative numbers of INP  $\text{mL}^{-1}$  of suspension estimated following Vali  
502 (1971) and Eq. 1. Conversion to ambient air concentrations  $\text{std L}^{-1}$  were made based on distributed  
503 suspension volume and the total air volumes collected (Eq. 2). Filter blanks were collected during  
504 FIN-03, one was tested and used to obtain background INP numbers per filter. Blank INPs were  
505 found to account for  $<5\%$  of INPs at  $-20$  and  $-25\text{ }^{\circ}\text{C}$ . Binomial sampling confidence intervals  
506 (95%) were derived for INP concentrations following Agresti & Coull (1998). The temperature  
507 uncertainty of INP measurements is  $\pm 0.2\text{ }^{\circ}\text{C}$ .

508 As a special contribution to FIN-03, portions of IS aerosol suspensions were set aside (e.g.,  
509 suspensions of 6 to 10 ml can serve up to three or more IS aliquot fills) for treatments to proximally  
510 isolate total biological, other organic and inorganic contributions to measured immersion freezing  
511 INP concentrations. To assess removal of heat labile INP entities, a 2 mL aliquot of suspension  
512 was re-tested in the IS after heating to  $95\text{ }^{\circ}\text{C}$  for 20 min (McCluskey et al. 2018). To attempt to  
513 remove all organic INPs, 1 mL of 30%  $\text{H}_2\text{O}_2$  was added to a 2 mL aliquot of suspension and the  
514 mixture heated to  $95\text{ }^{\circ}\text{C}$  for 20 min while illuminated with UVB fluorescent bulbs to generate  
515 hydroxyl radicals (residual  $\text{H}_2\text{O}_2$  is then removed using catalase) (Suski et al. 2018), and the INPs  
516 were again assessed for freezing spectra in the IS. Herein we describe a subset of samples collected  
517 on September 15, September 23, and September 25 that were subjected as IS suspensions to the  
518 two treatments. These treatments are based on well-established methods which have been used to  
519 assess biological components in samples for more than 60 years (Alsante et al., 2023, and  
520 references therein). The interpretation of data from exposure of particle suspensions to  $95\text{ }^{\circ}\text{C}$  is  
521 that the reduction of INP concentrations under thermal treatment is a proxy for the concentration  
522 of biological (proteinaceous and microbial) INPs which have been eliminated or deactivated



523 through treatment. A strong reduction in INP activity observed after peroxide treatment indicates  
524 dominant organic INP populations, whereas a lack of response to this treatment is assumed to  
525 indicate that inorganic INPs such as mineral dusts dominate non-heat labile INPs. This assessment  
526 for bulk suspensions of particles could be directly compared to measurements of 300C heat treated  
527 single particles in the online CSU CFDC measurements on these same days, providing a more  
528 insightful investigation of INP compositions.

529 The use of such treatments and the insights they convey for atmospheric ice nucleation  
530 studies has been reported in published studies of INPs for a variety of locations (McCluskey et al.,  
531 2018; Suski et al., 2018; Barry et al., 2021a; Knopf et al., 2021; Testa et al., 2021). Taken together,  
532 such treatment studies show general utility for estimating biological contributions to INP, overall  
533 organic contributions and the importance of inorganic contributions. However, we note that not all  
534 biological materials may be completely denatured or removed by heat (Testa et al., 2021; Daily et  
535 al., 2022; Alsante et al., 2023) and not all organics may be removed by peroxide. For example,  
536 denaturation is the disruption of higher order (secondary, tertiary, and quaternary structure) in a  
537 protein which leads to a loss or lessening of function. It follows that simpler proteins or peptides,  
538 such as glutathione, have no higher order structure, and thus cannot be denatured (Alsante et al.,  
539 2023). Consequently, estimates of biological contributions to INP based on these treatments may  
540 be considered as lower limits.

#### 541 FRIDGE Cold Stage and Deposition Nucleation Measurements

542 The FRIDGE instrument can be used to measure the concentration of INPs by two  
543 independent methods: a) a droplet freezing assay on a cold stage (hereafter: FRIDGE-CS Schrod  
544 et al., 2020; DeMott et al. 2018; Hiranuma et al. 2015) which addresses immersion freezing  
545 similarly to the NC State-CS and the CSU-IS and b) the diffusion chamber method (hereafter:





546 FRIDGE-DC), that addresses the deposition nucleation and condensation freezing modes  
547 introduced in Schrod et al. (2016) and referred to as the “standard” method in previous publications  
548 (e.g., DeMott et al, 2018). The ice nucleation analysis is performed inside the FRIDGE instrument  
549 for both methods, yet the sampling process, addressed nucleation modes and the specific analytical  
550 procedure differs as described below.

551 For the FRIDGE-CS method, aerosol particles were sampled via a short ¼” conductive  
552 tube from the shared turbulent flow aerosol inlet in the SPL instrument laboratory on Teflon  
553 membrane filters (Fluoropore PTFE, 47 mm, 0.2 µm, Merck Millipore Ltd.). The sampling  
554 duration ranged from 50 to 240 minutes, resulting in air volumes between 250 and 1000 std. L.  
555 The particles were extracted in 10 ml deionized water by shaking. Approximately 150, 0.5 µL  
556 droplets from that solution were pipetted onto a clean, silanized silicon wafer on the cold stage of  
557 the FRIDGE instrument and cooled by  $-1^{\circ}\text{C min}^{-1}$  at ambient pressure. A CCD camera detects  
558 freezing events and counts the number of frozen droplets as a function of temperature. This process  
559 is repeated with fresh droplets and fresh substrates until approx. 1000 droplets are attained. The  
560 INP number concentration is derived by Eqs. 1 and 2.

561 For the FRIDGE-DC measurements, an electrostatic aerosol collector EAC (Schrod et al.,  
562 2016) was connected to the same aerosol flow inlet via a short ¼” conductive tube. The EAC  
563 consists of a cylindrical sampler, whose inlet is concentrically surrounded by 12 gold wires that  
564 are at 12 kV against a grounded silicon wafer, which is used as the sample substrate, at the  
565 bottom of the sampler. Once the airflow is pumped inside, aerosol particles are charged by  
566 electrons emitted from the gold wires and are precipitated onto the silicon wafer. The analysis at  
567 certain pairs of T and RH follows in a separate step. For that, the wafer is placed on the cold  
568 stage inside a diffusion chamber. After the chamber is evacuated, the temperature is set to the



569 first analysis temperature. In a second, much larger volume, pure water vapor is regulated by  
570 pressure control to the desired supersaturation. Once the water vapor diffuses into the chamber,  
571 ice forms on the activated INPs and a CCD camera is used to record and count the emerging ice  
572 crystals, which appear as bright objects. It is assumed that one ice crystal represents one INP.  
573 The water vapor atmosphere and thus the growth of ice crystals is maintained for up to 100  
574 seconds until the valve to the water vapor source is closed and the chamber is evacuated again.  
575 The process is repeated at increasing humidity first, and then at progressively lower  
576 temperatures. At SPL samples were taken from the electrostatic sampler for 50, 75 and 120  
577 minutes, resulting in volumes of approximately 64-150 sL. The samples were analyzed by  
578 default at  $-20\text{ }^{\circ}\text{C}$ ,  $-25\text{ }^{\circ}\text{C}$  and  $-30\text{ }^{\circ}\text{C}$  and 95 %, 99% and 102% water saturation. In addition, a  
579 few samples were analyzed at  $-15\text{ }^{\circ}\text{C}$ . This was a special contribution by the FRIDGE group for  
580 comprehensive analysis of INP activation in the deposition regime, and for comparison to online  
581 data in this regime collected for some days.

### 582 **2.3 INP processing and sampling strategies**

583 As a campaign strategy, samples were collected over different time periods in the day to  
584 reflect both varied weather conditions and aerosol populations arriving at the mountain  
585 laboratory. For intercomparison, a select number of 4-hour sampling periods were allocated in  
586 which online instruments attempted to operate at a few predesignated temperature and relative  
587 humidity ranges, while samples were collected continuously for off-line analysis. While aerosol  
588 conditions can change within a 4-hour time frame, this was agreed upon as a minimal reasonable  
589 period for comparability. Similar sampling strategies have been employed in the past  
590 intercomparisons (DeMott et al., 2017; Knopf et al., 2021). Overall, measurements were  
591 conducted over a wide range of temperatures ( $-7$  to  $-34\text{ }^{\circ}\text{C}$ ) in the heterogeneous ice nucleation

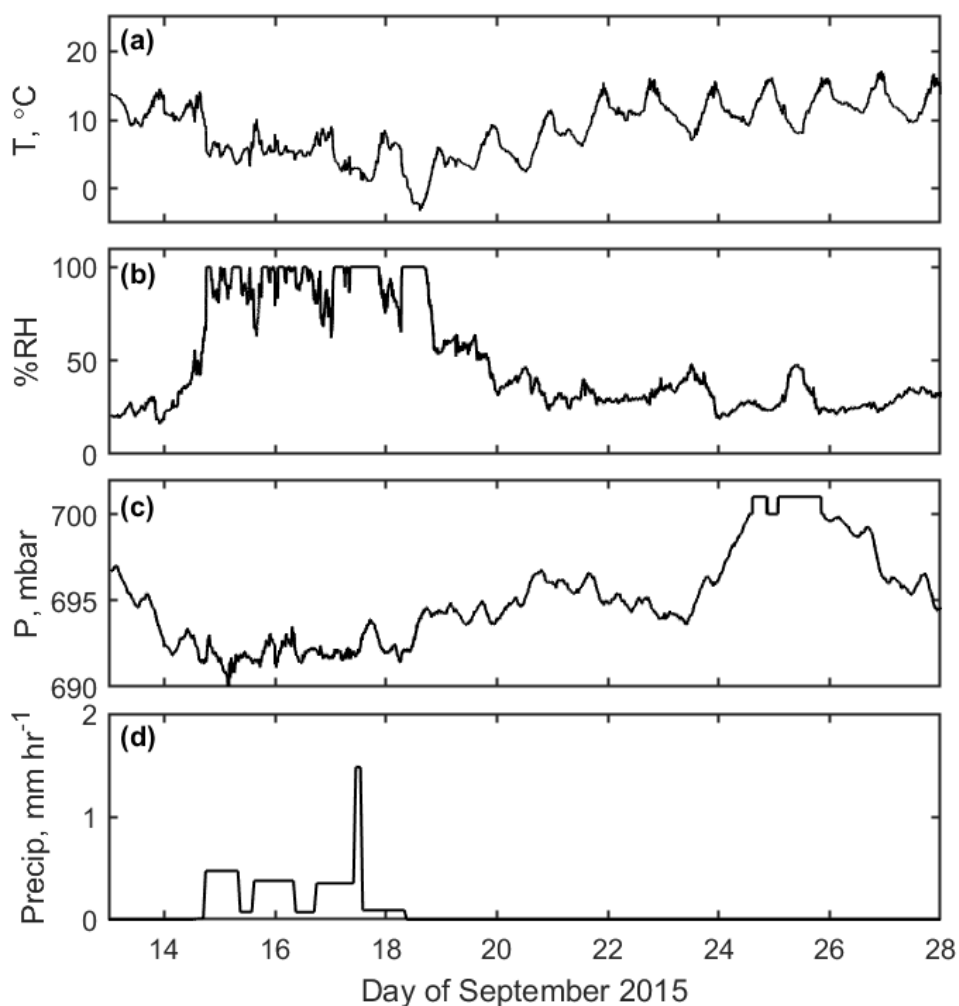


592 regime. Sampling such a broad data set allows for the consideration of instrument performance  
593 in response to the presence of highly active INPs (i.e., those facilitating freezing at temperatures  
594  $\geq -10$  °C) as well as more modestly effective INP ( $-10$  °C  $\geq T \geq -30$  °C). In addition, the range  
595 of INP concentrations includes lower concentrations which challenge instrumental limits of  
596 detection.

### 597 **3 Results and discussion**

#### 598 **3.1 Meteorological context**

599 Weather conditions during FIN-03 were characterized using auxiliary measurements.  
600 Weather data (temperature, humidity, winds and pressure) were obtained for Storm Peak  
601 Laboratory through the MesoWest ([https://mesowest.utah.edu/cgi-](https://mesowest.utah.edu/cgi-bin/droman/meso_base_dyn.cgi?stn=STORM)  
602 [bin/droman/meso\\_base\\_dyn.cgi?stn=STORM](https://mesowest.utah.edu/cgi-bin/droman/meso_base_dyn.cgi?stn=STORM)) mesonet (STORM site), supplemented with  
603 measurements from instruments operated at SPL through the Western Regional Climate Center  
604 (WRCC) (<https://wrcc.dri.edu/weather/strm.html>) for the two days that were absent in the  
605 MesoWest record. Air temperature, relative humidity, and barometric pressure time series are  
606 shown in Figure 1(a), 1(b) and 1(c), respectively. Precipitation was measured via a rain gauge at  
607 Storm Peak Laboratory provided by NC State. Precipitation rate was calculated from the quotient  
608 of precipitation (in mm) and time collected (in hours), as shown in Figure 1(d). Back trajectories  
609 for all the sampling days in FIN-03 are reported by Zawadowicz et al. (2017), showing 72-hr air  
610 mass transits from regions that included Southern California, Washington State and Eastern  
611 Nebraska.



612

613 **Figure 1.** Weather conditions over the course of FIN-03, including (a) air temperature, (b) relative

614 humidity, (c) barometric pressure, and (d) precipitation rate.

615

616 Relatively warm, dry conditions were observed initially at the Storm Peak Laboratory.

617 Clear skies on September 11 and 12, 2015 gave way to clouds and haze on September 13.

618 Cooler temperatures, lower barometric pressure, and higher relative humidity (generally above >



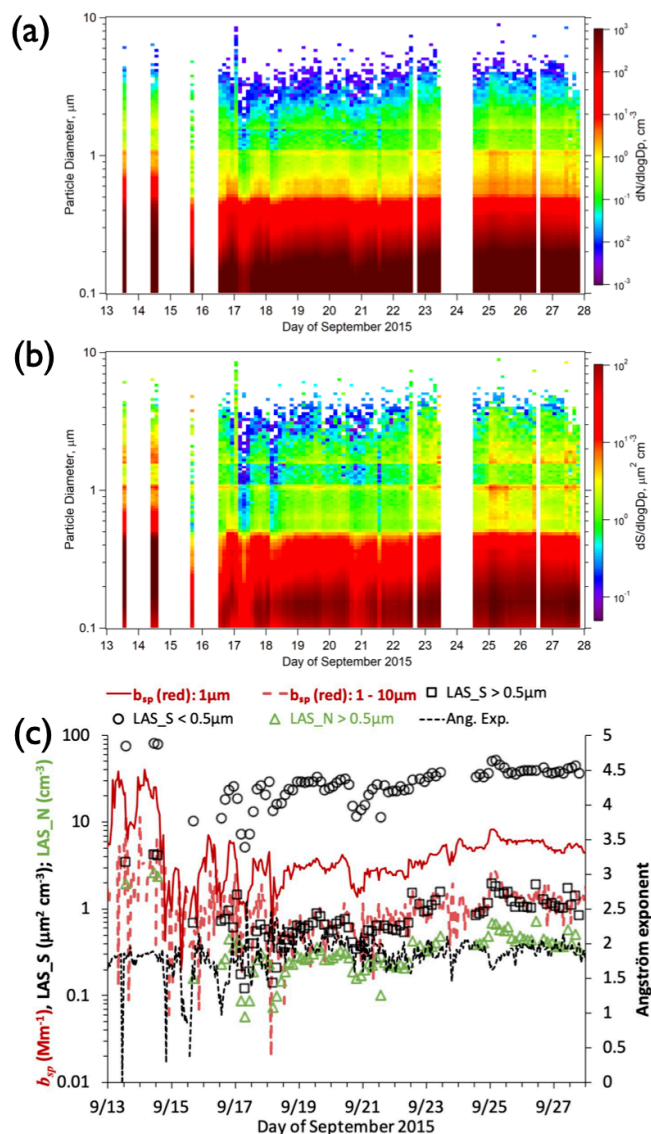
619 70%) accompanied rainfall on September 14. This was followed by continued rain on September  
620 15, intermittent rain and short periods of hail on September 16, a mixture of rain, snow, and sleet  
621 on September 17, and snow on September 18. The next and longest period in the study,  
622 September 19 to 28, was marked by an increase in temperature, an increase in barometric  
623 pressure, lower relative humidity, and a lack of precipitation. More detailed weather records  
624 including daily photographs and a summary of human-produced daily observations are  
625 summarized in supplemental Section S1. Daily wind rose plots are provided in Figure S1.

## 626 **3.2 Aerosol context**

### 627 **3.2.1 Aerosol size distribution and surface area**

628 The time series of aerosol size distribution measured by the LAS (in three hour means) is  
629 shown in Figure 2a. The maximum and minimum total LAS concentrations were  $706 \text{ cm}^{-3}$  and  
630  $74 \text{ cm}^{-3}$  respectively, and the mean and standard deviation of the total LAS concentration  
631 throughout FIN-03 were  $410 \text{ cm}^{-3}$  and  $138 \text{ cm}^{-3}$ , respectively. The highest total LAS  
632 concentration recorded during FIN-03 ( $706 \text{ cm}^{-3}$ ) occurred in the early hours on September 25.  
633 Elevated aerosol concentration (at least one standard deviation above the mean) was also  
634 observed during midday on September 13, before and during midday on September 14, before  
635 midday on September 25, in the afternoon on September 26, and around midday on September  
636 27.

637 The timeline of LAS aerosol surface area in Figure 2b emphasizes that surface area was  
638 predominately submicron throughout the study, with a mode at about  $0.16 \mu\text{m}$ . This is important  
639 to note, in combination with chemical composition information discussed in the next section  
640 because it is relevant to understanding the likely sizes and surface areas of INPs. We will revisit  
641 the surface area of INPs for use in parameterizations in a later section. Quantitative timelines of



642

643 **Figure 2.** Time series of dry particle number concentration distribution (ambient conditions, not STP)

644 measured by the laser aerosol spectrometer (LAS) in a), shown as three-hour means at ambient pressure.

645 Time series of particle surface area distribution is in b). Timeline of nephelometer scattering (1-hr data) in

646 the red channel for  $< 1 \mu\text{m}$  and  $1 - 10 \mu\text{m}$  size ranges, 3-hr LAS number concentration  $> 0.5 \mu\text{m}$ , 3-hr

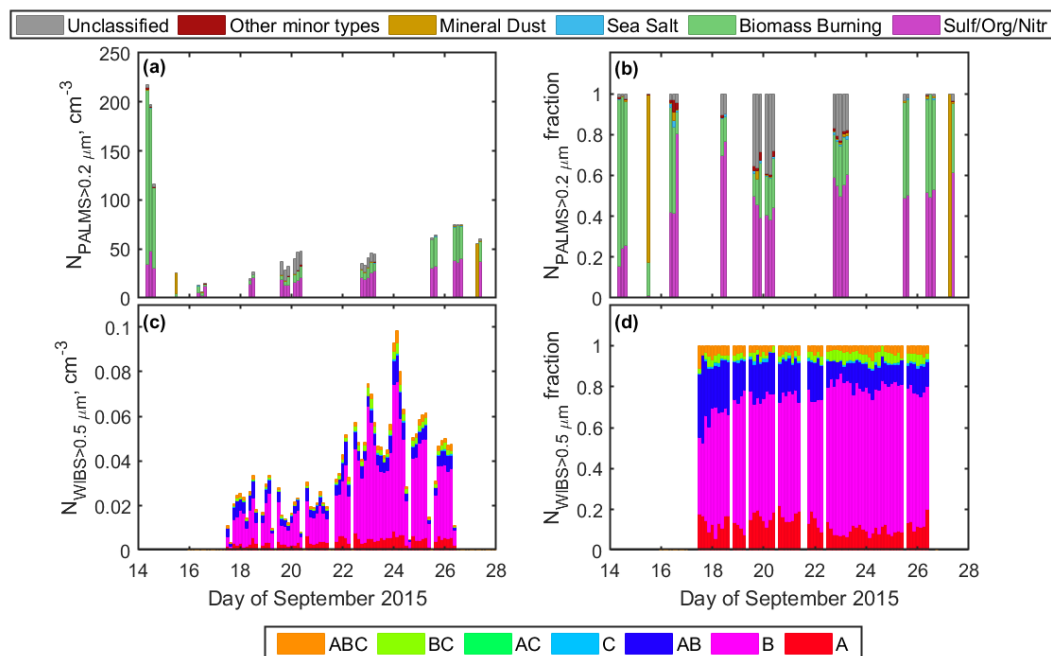
647 LAS surface area at sizes below and above  $0.5 \mu\text{m}$ , and Angström exponent (dashed, right axis).



648 LAS surface area above and below 0.5  $\mu\text{m}$  are shown in Figure 2c. Surface area at above 0.5  $\mu\text{m}$   
649 is about a factor of 30 lower than at below this size over most of the study period. Also shown in  
650 Figure 2c is nephelometer scattering ( $b_{sp}$ ) in the red channel (700 nm) showing a dominant  
651 contribution when the upstream impactor was set to 1  $\mu\text{m}$  (aerodynamic) and a much lower level  
652 of 1 – 10  $\mu\text{m}$  scattering. This scattering from coarse mode particles is consistent with and trends  
653 with the LAS surface area in the supermicron regime, while the Angström exponent (calculated  
654 using red and blue channels) being close to 2 (small particle dominance) throughout the study is  
655 consistent with the dominance of submicron contributions to total surface area. Figure 2 also  
656 emphasizes that the lowest aerosol concentrations and surface areas occurred during varied time  
657 in the wet period of the study from midday on the 14<sup>th</sup> through the 17<sup>th</sup> of September.

### 658 **3.2.2 Aerosol composition**

659 The number concentration of aerosol particles from 0.2 to 3  $\mu\text{m}$  with characteristic  
660 spectra belonging to eight composition categories (sulfate/organic/nitrate, biomass burning,  
661 elemental carbon, sea salt, mineral dust, meteoric, alkali salt, and fuel oil combustion), and the  
662 number concentration of unclassified aerosol particles by the PALMS, were assessed for three-  
663 hour averages through the FIN-03 period. For simplicity, four of these categories (elemental  
664 carbon, meteoric, alkali salt, and fuel oil combustion) were combined into a category called  
665 “other” due to the low concentration of particles in each of these categories resulting in 6 total  
666 classifications (categories (SulfOrgNit = sulfates/organics/nitrates, BioBurn = products of  
667 biomass burning, Sea salt, Mineral dust, and Unclassified), as shown in Figure 3a. The three-  
668 hour averages of the number fractions of each particle type were also calculated as the fraction of  
669 the total aerosol number concentration measured by the PALMS in each of the six  
670 classifications, as shown in Figure 3b. The dominant categories throughout the FIN-03

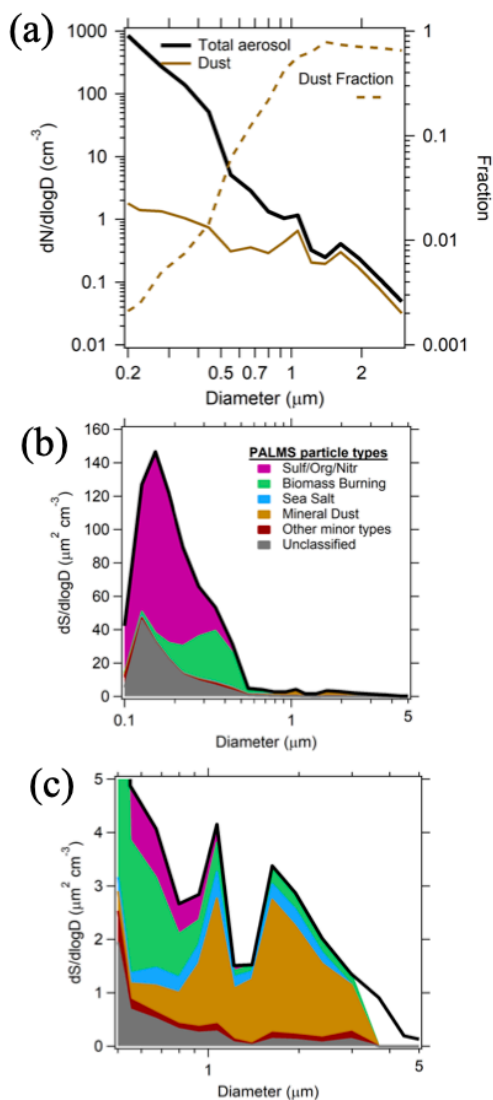


671

672 **Figure 3.** Subplots (a) and (b) show the aerosol particle number (ambient conditions, not STP) and  
 673 relative fractions (by cumulative count at all sizes) of each of the six PALMS compositional particle types  
 674 for the three-hour periods during which the PALMS was used to sample ambient air. Subplots (c) and (d)  
 675 show the aerosol particle number concentration and relative fractions (by count) of particles with diameter  
 676  $> 0.5 \mu\text{m}$  in each of the channels (A, B, AB, C, AC, BC, and ABC, which are described in Perring et al.,  
 677 2015) over the course of the FIN-03 field campaign.

678





679

680 **Figure 4.** a) Total aerosol versus mineral/soil dust (ambient) number size distribution and dust fraction

681 interpreted from PALMS and LAS data for all times that the PALMS was sampling during FIN-03. b)

682 Surface area distribution differentiated for PALMS compositional types during the same sampling times.

683 c) Expanded plot from b) for the coarse mode size range to emphasize progressive dominance of dust

684 components at diameters  $> 0.5 \mu\text{m}$ .



685 campaign were BioBurn (mean  $26 \pm 43 \text{ cm}^{-3}$ , maximum  $177 \text{ cm}^{-3}$ ), SulfOrgNit (mean  $22 \pm 13$   
686  $\text{cm}^{-3}$ , maximum  $48 \text{ cm}^{-3}$ ), and mineral dust (mean  $3 \pm 11 \text{ cm}^{-3}$ , maximum  $55 \text{ cm}^{-3}$ ). The mineral  
687 dust type also includes soil particles (crustal species mixed with organic material) (Zawadowicz  
688 et al., 2019). The highest total particle number concentration measured by the PALMS ( $218$   
689  $\text{cm}^{-3}$ ) occurred on September 14 (of which  $177 \text{ cm}^{-3}$  consisted of biomass burning and  $34 \text{ cm}^{-3}$   
690 consisted of sulfates/organics/nitrates). This biomass burning plume impacted the site for several  
691 hours. Mineral/soil dust particles were ubiquitous throughout the study, with a concentration of  
692  $0.128 \pm 0.446 \text{ cm}^{-3}$  (median and interquartile range). Anomalous concentrations  $>10 \text{ cm}^{-3}$   
693 observed for a few 5-min sample periods are likely due to road dust emitted from site. Dust  
694 concentrations were  $<1 \text{ cm}^{-3}$  for 90% of the PALMS samples. Mineral/soil dust represented a  
695 median of 0.3% of particles in the  $>0.2 \mu\text{m}$  size range, increasing to 23% and 67% for  $>0.5$  and  
696  $>1.0 \mu\text{m}$  particles (Figure 4a). Similarly, mineral dust contributions to total surface area are  
697 inconsequential for total aerosol (Figure 4b) but dominate in the coarse mode regime for the  
698 study (Figure 4c). We will revisit this result in discussions of parameterization of INPs in Section  
699 3.5.

700 The daily average number concentration of fluorescing aerosol particles corresponding  
701 with each of the seven WIBS-4A types with diameter  $> 0.5 \mu\text{m}$  is shown in Figure 3(c), and the  
702 daily average number fraction of each WIBS-4A type is shown in Figure 3(d). The dominant  
703 types of fluorescent aerosol particles throughout the FIN-03 field campaign were types B, AB,  
704 and A, which on average accounted for  $63.2\% \pm 8.7\%$ ,  $16.0\% \pm 6.3\%$ , and  $12.5\% \pm 3.9\%$  of the  
705 particles detected by the WIBS respectively.

706 In contrast with the daily average number fraction in each PALMS category, the relative  
707 contributions of each of the seven WIBS-4A particle types did not vary much over the course of

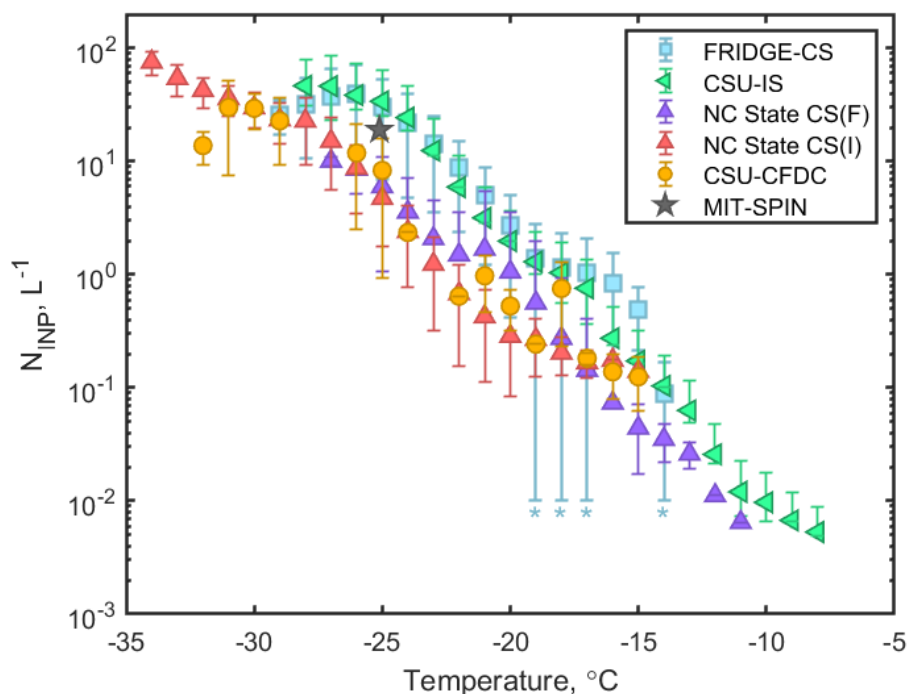


708 the study when the WIBS-4A was operational, with perhaps the exception that Type AB  
709 decreased in prevalence from September 18 (42.9%) to September 21 (10.1%). A modest trend  
710 from lower total fluorescing particle concentrations ( $0.02$  to  $0.04$   $\text{cm}^{-3}$  at STP) through  
711 September 21 to higher concentrations ( $0.07$  to  $0.15$   $\text{cm}^{-3}$  at STP) from September 22 through  
712 26<sup>th</sup>. WIBS-4A data was not collected on September 13-16, nor on September 27. The first  
713 period was somewhat critical to evaluating INP relations to bioaerosols, so we note here in  
714 advance this caveat. Time-resolved size distributions for each WIBS-4A channel, as well as the  
715 total particle concentration measured across these seven channels, are shown in supplemental  
716 Figure S2. FBAP assignments related to INP predictions will be discussed in Section 3.5.

### 717 **3.3 Immersion freezing measurements**

718 A summary of the number concentrations of immersion freezing INPs ( $N_{\text{INP}}$ ) over the  
719 course of the field campaign, binned for one degree temperature intervals, is shown in Figure 5.  
720 The concentration of INP detected over this range ranged over five orders of magnitude ( $0.01$  to  
721  $160$   $\text{L}^{-1}$ ). At any one temperature, differences up to a little more than one order of magnitude are  
722 apparent in comparing average data from individual methods, mirroring results presented in  
723 previous laboratory and field studies (Hiranuma et al., 2015; DeMott et al., 2017, 2018; Knopf et  
724 al., 2021; Lacher et al., 2024).

725 As expected, a trend of increasing  $N_{\text{INP}}$  with decreasing temperature was observed for the  
726 FRIDGE-CS, CSU-IS, NC State-CS, and CSU-CFDC. The data represented by the single MIT-  
727 SPIN processing temperature condition also falls well within the concentration range reported for  
728 the other instruments. Incremental changes in  $N_{\text{INP}}$  with decreasing temperature was similar for  
729 all measurements that spanned a broad temperature range. This comparability of  $dN_{\text{INP}}/dT$   
730 contrasts with an apparent increasing high bias of drop suspension freezing measurements versus



731

732 **Figure 5.** Campaign average immersion freezing INP concentrations ( $sL^{-1}$ ) in  $1\text{ }^{\circ}C$  bins for instruments  
 733 participating in intercomparison studies. Error bars represent one standard deviation in the measurement  
 734 means collected at the specified temperature and not measurement uncertainties. The star labels indicate  
 735 when these exceeded the mean for the FRIDGE-CS data. The times over which the INP concentration has  
 736 been averaged for each instrument is explained in the text.

737

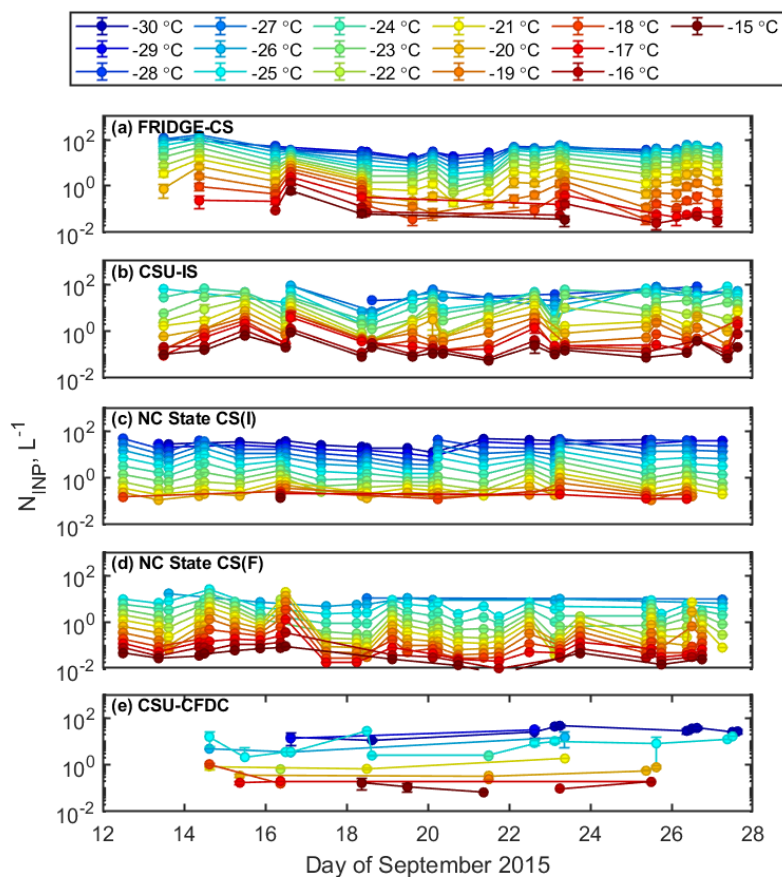
738 CFDC measurements during comparable sampling at various surface sites (non-mountaintop or  
 739 free troposphere) found in DeMott et al. (2017) but agrees with FIN-02 laboratory studies  
 740 (DeMott et al., 2018) and recent atmospheric studies at Puy de Dome (Lacher et al., 2024). INP  
 741 concentration variability at single temperatures, reflected in Figure 5 as a standard deviation of  
 742 bin means, is likely due to variations in aerosol properties in response to production and  
 743 scavenging processes upstream of the site. Nevertheless, generally higher  $N_{INP}$  measurements



744 were obtained with the FRIDGE-CS and the CSU-IS than the CSU-CFDC and NC State-CS (F)  
745 and NC State-CS (I) analyses. Such biases in other studies have been attributed to different  
746 efficiencies in sampling of largest particles (e.g., Lacher et al., 2024; Cornwell et al., 2023), but  
747 the collection methods for offline measurements in this study were substantially similar, as  
748 discussed further below. Hence, we cannot attribute measurement differences to a systematic  
749 source. Comparability of impinger versus filter sampling methods for immersion freezing  
750 measurements via the NC State-CS mirrors the findings in DeMott et al. (2017).

751 To compare the operation of these instruments over time, the mean and standard  
752 deviation (when applicable) of immersion freezing  $N_{\text{INP}}$  were calculated over three-hour periods  
753 for each instrument (except for the MIT-SPIN) at 1 °C intervals ( $\pm 0.5$  °C). Means are plotted as  
754 a time series in Figure 6. Although some differences appear in comparing instrument by  
755 instrument, as will be discussed, some general observations from the temporal data of Figure 6  
756 are that INP concentrations at temperatures  $> -20$  °C were at a maximum during the precipitation  
757 period, as might be expected for rainfall production of biological INPs (Huffman et al., 2013;  
758 Mignani et al., 2021; Testa et al., 2021; Cornwell et al., 2023), while the strongest differences  
759 between the concentrations of INPs active at higher and lower temperatures occurred during  
760 period of warming under high pressure later in the study. The latter observation might be  
761 expected for a strong contribution of dust-like INPs, with a steeper  $dN_{\text{INP}}/dT$ .

762 Periods of agreement and discrepancy are clearer in examining the ratios of time-matched  
763 and temperature-matched three-hour immersion  $N_{\text{INP}}$  values that were calculated for each pair of  
764 instruments, as shown in Figure 7. As a positive note, the mean  $N_{\text{INP}}$  reported by different  
765 instruments for all temperature conditions taken together generally fell within a span of one order  
766 of magnitude. Figure S3 shows the percent of immersion INP measurements in which all



767

768 **Figure 6.** Time series of immersion-freezing mode INP concentrations ( $\text{sL}^{-1}$ ) measured during

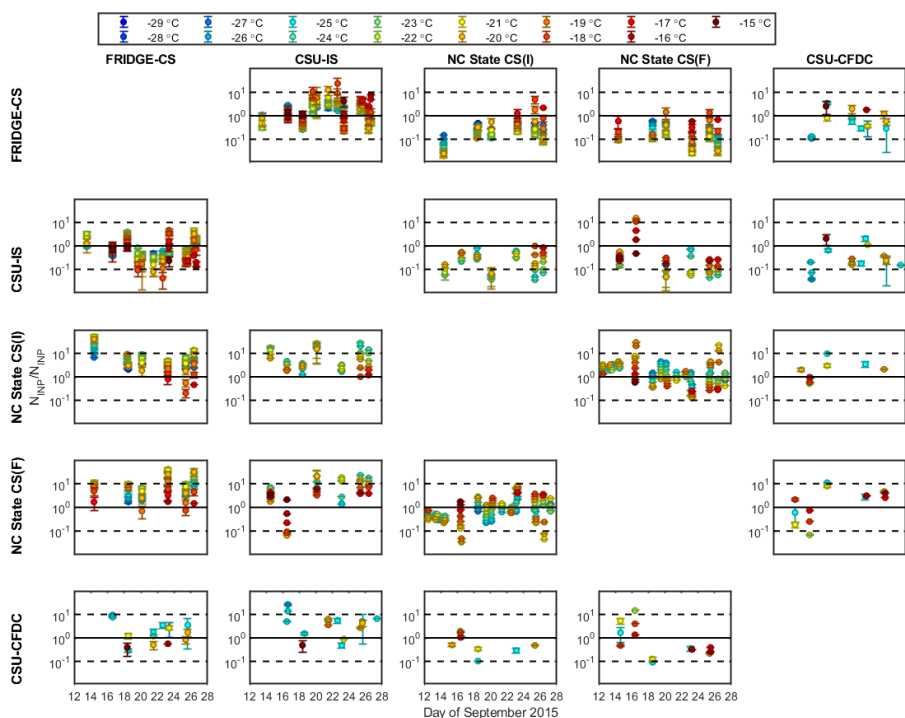
769 intercomparison periods by (a) the FRIDGE from Goethe University Frankfurt, (b) the CSU ice

770 spectrometer, (c) the NC State cold stage (collected using an impinger), (d) the NC State cold stage

771 (collected using the filter), and (e) the CSU continuous flow diffusion chamber. INP concentrations

772 shown in this figure are averaged over three-hour periods.

773



774

775 **Figure 7.** Ratios of the immersion freezing INP concentrations measured by each instrument, to the  
 776 immersion INP concentrations measured by each other instrument (three-hour averages). Each instrument  
 777 (FRIDGE, CSU-IS, NCSU-CS (I), NCSU-CS (F), and CSU-CFDC) is represented by one of the five  
 778 columns as well as one of the five rows.

779

780 instrument pairs agreed within one order of magnitude. This level of agreement compares well  
 781 with the findings from FIN-02, for which the immersion  $N_{INP}$  measured by several online and  
 782 offline instruments agreed within an order of magnitude. This is encouraging given that FIN-02  
 783 was a laboratory intercomparison on single composition aerosol samples consisting of particles  
 784 with diameter  $< 2 \mu\text{m}$  whereas FIN-03 was a field campaign in which constant changes in the  
 785 concentration, size distribution, and composition of the ambient aerosol population at Storm



786 Peak Laboratory were all potential factors. This shows that field data can be collected with  
787 nearly the same level of accuracy as laboratory experiments. While also mimicking the results of  
788 DeMott et al. (2017) for a smaller instrument comparison exercise, agreement was slightly  
789 poorer than found in another recent intercomparison where INP concentrations were stated to  
790 match within a factor of 5 (Lacher et al., 2024).

791 Reiterating what is apparent from campaign-wide results in Figure 5, the best agreement  
792 for short-term periods throughout the study as shown in Figure 7 was observed between the  
793 FRIDGE-CS and the CSU-IS, in which only one out of seventy-two 3-hour, time- and  
794 temperature-matched  $N_{\text{INP}}$  (1.4%) did not agree within an order of magnitude. Nevertheless,  
795 discrepancies of a few to several times did occur from September 19<sup>th</sup> onward, focused more  
796 often at  $>-22^{\circ}\text{C}$ , with the CSU-IS measuring higher from the 19<sup>th</sup> to the 22<sup>nd</sup> and the FRIDGE-  
797 CS higher at some other times, notably the 23<sup>rd</sup> and 26<sup>th</sup> of September. None of these periods  
798 were distinguished in any discernible manner by weather or aerosol properties. For example,  
799 LAS and PALMS concentrations were no more than 20% different than the FIN-03 campaign  
800 means during any of these periods. Aerosol surface areas were about a factor of two lower  
801 overall during the 19<sup>th</sup> to 22<sup>nd</sup> period than for the period after the 23<sup>rd</sup> (Figure 2), which does not  
802 imply a special sampling bias for larger particles for the IS filter that was open to the air, a point  
803 we will discuss further below.

804 Both the FRIDGE-CS and CSU-IS showed high bias from a few to more than 10 times  
805 versus NC State-CS(I) or CS(F), primarily at processing temperatures below  $-20^{\circ}\text{C}$ , whereas  
806 agreement was generally very much better at  $>-20^{\circ}\text{C}$ . The poorest agreement overall was  
807 observed for the CSU-IS compared to the NC State-CS(I), a combination for which 12 out of 44  
808 (27%) immersion  $N_{\text{INP}}$  means did not agree within an order of magnitude. Agreement between





809 the FRIDGE-CS and the NC State-CS(I) was only slightly better, as 13 out of 52 (25%) time-  
810 matched  $N_{\text{INP}}$  means did not agree within an order of magnitude. Higher than order of magnitude  
811 such discrepancies at lower temperatures were markedly present on September 14, 23 and 26.  
812 Based on PALMS data, the 14<sup>th</sup> was richer in compounds from biomass burning, poorer in  
813 sulfates, organics, and nitrates, and slightly poorer in mineral dust than average, as discussed in  
814 Section 3.2. The concentration of  $> 0.5 \mu\text{m}$  particles measured by the LAS during this time was  
815 also relatively high ( $2.5 \text{ cm}^{-3}$  compared to the campaign mean  $0.45 \pm 0.62 \text{ cm}^{-3}$ ). However, the  
816 14<sup>th</sup> is not markedly distinguished overall in the timeline of all INP measurements in Figure 6, so  
817 perturbations to composition and concentrations of all particle sizes due to the biomass burning  
818 event did not appear to specially perturb the INP populations. We have already noted that the  
819 23<sup>rd</sup> and 26<sup>th</sup> of September had aerosol populations that were not much different than the project  
820 mean on those days.

821         The CSU-CFDC INP measurements generally agreed with the other measurements within  
822 an order of magnitude for data collected on the same day and temperature, and its measurements  
823 of INP concentration were in best agreement with all methods for temperatures  $> -20 \text{ }^\circ\text{C}$ . CSU-  
824 CFDC INP concentrations tended to be lower than those from the FRIDGE-CS and CSU-IS at  
825 temperatures below  $-20 \text{ }^\circ\text{C}$ . A similar divergence in online versus offline  $N_{\text{INP}}$  measurements in  
826 this temperature range was reported by DeMott et al (2017) for ground-based sampling, with  
827 online measurements tending to measure progressively lower INPs than offline integrated filter  
828 or impinger collections at below  $-20 \text{ }^\circ\text{C}$ , approaching one order of magnitude below  $-25 \text{ }^\circ\text{C}$ . At  
829 the Puy de Dome mountain station (Lacher et al. 2024), only modest and insignificant  
830 underestimates were made by the CSU-CFDC (again, with a  $2.5 \mu\text{m}$  impactor) versus offline  
831 INP concentrations when all were measured from a PM10 inlet. CSU-CFDC INP measurements



832 were comparable on average with measurements from the NC State-CS(I) and NC State-CS(F),  
833 consistent with the mean results shown in Figure 5. Comparing the timeline of ratios of NC  
834 State-CS(I) to NC State-CS(F), only 5 out of 130 (4%) of the INP concentrations obtained  
835 through analysis by the identical off-line apparatus differed by more than an order of magnitude.

836 A possible explanation for INP measurement discrepancies that has been tendered in  
837 other intercomparison campaigns sampling ambient air is that INPs are highly sensitive to the  
838 size range of collected aerosol, and systematic size-dependent differences in collection  
839 efficiencies vary for different collection types (DeMott et al., 2017; Knopf et al., 2021; Lacher et  
840 al., 2024). For example, Lacher et al. (2024) found significant underestimates of INPs by both  
841 online and offline methods measuring from the PM10 inlet versus offline measurements from  
842 filter collections made on the laboratory rooftop. In this study, as we have noted above, a  
843 similarly consistent difference between rooftop versus laboratory or between online and offline  
844 measurements is not found. FRIDGE-CS measurements from the turbulent-flow inlet and CSU-  
845 IS measurements from the rooftop filter agreed on average over the course of the study. CFDC  
846 INP measurements agreed reasonably well with the NC State (F) and (I) measurements. Larger  
847 particles do tend to have higher ice nucleation efficiency, so biases in their collection can lead to  
848 sometimes large differences in assessed INP concentrations (Mason et al., 2016). Disaggregation  
849 of the very largest collected particles when placed in water suspensions has also been implicated  
850 for discrepancies between different substrate collections (DeMott et al., 2017; Lacher et al.,  
851 2024). An obvious size-based collection bias existed for the online INP instruments, which had  
852 impactors upstream to limit particles  $>2.5 \mu\text{m}$  (50% cut-size) from entering. There may have  
853 been additional line losses for these instruments sampling from an inlet and using tubing to  
854 transfer particles, though these tend to be of minor influence at below the impactor size cut



855 (Knopf et al., 2021). The impinger is known to be less efficient for small (<200 nm) and large  
856 (>10  $\mu\text{m}$ ) particle capture, but unless the relatively light to moderate wind conditions at the inlet  
857 during FIN-03 conferred some special bias, Hader et al. (2014) predict a 50% capture efficiency  
858 at near 10  $\mu\text{m}$ . The filter samplers on the rooftop should have been equivalent, with the only  
859 difference in the orientation of filters for the NC State samples being mounted face-down. The  
860 size bias in this configuration is unknown. The FRIDGE filter should have captured particles  
861 with the same efficiency as the turbulent flow inlet, since only a very short line connected the  
862 filter to the interior inlet structure in the laboratory. Only if very large INPs > 13  $\mu\text{m}$  were  
863 dominant by number amongst total INPs, which is unexpected, would the FRIDGE filter  
864 collection have been expected to differ from the rooftop filter collections.

865 In the end, it seems more likely that unquantifiable random and non-random sources of  
866 discrepancy, related to such things as sample size, instrument temperature sensor drift, varied  
867 instrument cooling rates and inconsistency in sample materials or handling and storage (e.g.,  
868 Barry et al., 2021b; Beall et al., 2021), may also contribute to the fact that measurements of  
869 immersion freezing INP concentrations from ambient air are generally uncertain by up to one  
870 order of magnitude, as this study once again supports.

### 871 **3.4 Relation of immersion freezing INPs to aerosol properties**

872 While establishing correlations between INPs and aerosol properties were not a focus of  
873 the intercomparison, the ancillary aerosol data did allow for inspecting some simple linear  
874 correlation analysis. This provides insight into the size range of greatest relevance for the INP  
875 intercomparison period. Throughout the campaign, a positive and significant trend between total  
876 LAS particle concentration (i.e., > 0.1  $\mu\text{m}$ ) and  $N_{\text{INP}}$  was observed for FRIDGE-CS ( $R = 0.55$ -  
877 0.74 and  $p < 0.05$  for measurements at  $-28\text{ }^\circ\text{C} < T < -15\text{ }^\circ\text{C}$ ), but no clear statistically significant



878 trend was observed between total LAS particle concentration and  $N_{\text{INP}}$  for the other four  
879 instruments (Figure S4a). A greater number of significant positive trends were found between the  
880 concentration of particles with diameter  $> 0.5 \mu\text{m}$  and  $N_{\text{INP}}$ . This was the case for the FRIDGE-  
881 CS ( $R = 0.54-0.94$  and  $p < 0.05$  for measurements at  $-28 \text{ }^\circ\text{C} < T < -19 \text{ }^\circ\text{C}$ ), CSU IS ( $R = 0.46-$   
882  $0.72$  and  $p < 0.05$  for measurements at  $-21$  to  $-25 \text{ }^\circ\text{C}$ ), NC State CS(I) ( $R = 0.46-0.61$  and  $p <$   
883  $0.05$  for measurements at  $-29 \text{ }^\circ\text{C} < T < -24 \text{ }^\circ\text{C}$ ), and the NC State CS(F) ( $R = 0.51-0.64$  and  $p <$   
884  $0.05$  for measurements at  $-26 \text{ }^\circ\text{C} < T < -22 \text{ }^\circ\text{C}$ ).

885 No consistent, significant ( $p < 0.05$ ) correlation was found between changes in  
886 composition (from the PALMS categories and WBS-4A types) and immersion freezing  $N_{\text{INP}}$   
887 across the range of setpoint temperatures employed during FIN-03 (Figure S4b).

### 888 **3.5 Inferences to INP compositions during FIN-03**

889 To provide context for the discussed intercomparisons and because this study provides  
890 data needed for testing the relevance of existing parameterizations of ice nucleation in regional  
891 and global climate models (Andreae & Rosenfeld, 2008; Morris et al., 2011; Seifert et al., 2011),  
892 we utilize some previously-developed ice nucleation parameterizations for specific compositions  
893 to diagnose consistency or not with INP compositions in the high altitude environment of FIN-  
894 03. We examine parameterizations for mineral dust INPs that have different links to larger size  
895 particle concentrations (DeMott et al., 2015) versus mineral dust surface area (Niemand et al.,  
896 2012), and biological INPs as linked to fluorescent particle concentrations (Tobo et al., 2013;  
897 Twohy et al., 2016). Hereafter we will refer to these parameterizations as DeMott 2015,  
898 Niemand 2012, and Tobo 2013. We also utilize a more direct method of probing INP  
899 compositions using the IS sample treatments discussed in Section 2.2.2.



900 Each of the above-noted deterministic parameterizations was used to predict  $N_{\text{INP}}$  at  $-30$   
901  $^{\circ}\text{C}$ ,  $-25$   $^{\circ}\text{C}$ ,  $-20$   $^{\circ}\text{C}$ , and  $-15$   $^{\circ}\text{C}$  using the equations and inputs described in Table 2 and  
902 summarized below. We do not attempt an analysis using stochastic parameterizations.

903 1) DeMott 2015 is based on CSU-CFDC laboratory measurements of ice nucleation on  
904 mineral dust soil samples as well as field data from situations dominated by mineral dusts  
905 (i.e., dust plumes from major deserts), collected for CFDC operational conditions  
906 essentially the same as for this study (i.e., simulated immersion freezing conditions at  
907 105% RH) (DeMott et al., 2015). For FIN-03, aerosol concentrations measured by the  
908 LAS ( $> 0.5$   $\mu\text{m}$  dry diameter) and converted to STP concentrations were used as the input  
909 for this parameterization for comparison to INP data that is also reported at STP  
910 concentrations. Predictions also depend on temperature (Table 2). Since PALMS data  
911 indicates that dust particles dominated the coarse mode only at sizes above 1  $\mu\text{m}$  in  
912 diameter (Figure 4), we first adjust LAS data accordingly for the percentage of dust  
913 particles with diameters  $> 0.5$   $\mu\text{m}$  as input to this parameterization, which we have  
914 already stated is 23%. A correction factor (CF) of 3 was also applied (as indicated in  
915 Table 2) according to the results in DeMott et al. (2015) which showed that when  
916 applying the parameterization to represent immersion freezing INP concentrations in a  
917 model or in comparison to other immersion freezing methods, this CF is needed to  
918 account for CFDC underestimates of immersion freezing INPs (see Methods). The CF is  
919 applied in this case because calculations will be compared to the average  $N_{\text{INP}}$  from all  
920 measurements.

921 2) The Niemand 2012 parameterization (Table 2) for mineral dust INPs is based entirely  
922 from laboratory measurements and incorporates measurements of temperature and



923 particle surface area as the basis for prediction of INPs. It is especially important to limit  
 924 the size range of aerosols for which this parameterization is applied, because total surface  
 925 area was dominated by small particles in FIN-03. Therefore, with reference to Figure 4,  
 926 we will assume that all dust surface area occurs at sizes larger than 0.5  $\mu\text{m}$  and represents  
 927 50% of that surface area.

928 **Table 2** Summary of INP parameterizations.

Parameterization	Equation	Constants
Mineral dust INPs: Niemand et al. (2012)	$N_{INP}(T_C) \approx n_s(T_C)S_{tot} = (a \exp(b(T_C) + c))(S_{tot})$ $N_{INP}(T_C) = \text{INP concentration (sL}^{-1}\text{) at T (Celcius)}$	$a = 1 \times 10^{-9}$ $b = -0.515$ $c = 8.821$
Mineral dust: DeMott et al. (2015)	$N_{INP}(T_K) = (cf)(n_{a>0.5\mu m})^{(\alpha(273.16-T_K)+\beta)}$ $\exp(\gamma(273.16 - T_K) + \delta)$ $N_{INP}(T_K) = \text{INP concentration (sL}^{-1}\text{) at T (Kelvin)}$ $n_{a>0.5\mu m} = \text{mineral particle number concentration } > 0.5 \mu\text{m (scm}^{-3}\text{)}$ $cf = 1 \text{ (CFDC data comparison) or } 3 \text{ (other immersion freezing)}$	$\alpha = -0.074$ $\beta = 3.8$ $\gamma = 0.414$ $\delta = -9.671$
Fluorescing biological aerosol particle INPs: Tobo et al. (2013)	$N_{INP}(T_k) = (N_{FBAP>0.5\mu m})^{(\alpha'(273.16-T_k)+\beta')}$ $\exp(\gamma'(273.16 - T_k) + \delta')$ $N_{INP} = \text{INP concentration (sL}^{-1}\text{)}$ $N_{FBAP} = \text{FBAP concentration (scm}^{-3}\text{)}$	$\alpha' = -0.108$ $\beta' = 3.8$ $\gamma' = 0$ $\delta' = 4.605$
Fluorescing biological aerosol particle INPs: Cornwell et al. (2023)	$N_{INP}(T_C) = f(T_C)1000N_{FBAP>0.5\mu m}$ $f(T_C = -20 \text{ }^\circ\text{C}) = 0.318$ $f(T_C = -15 \text{ }^\circ\text{C}) = 0.016$	N/A

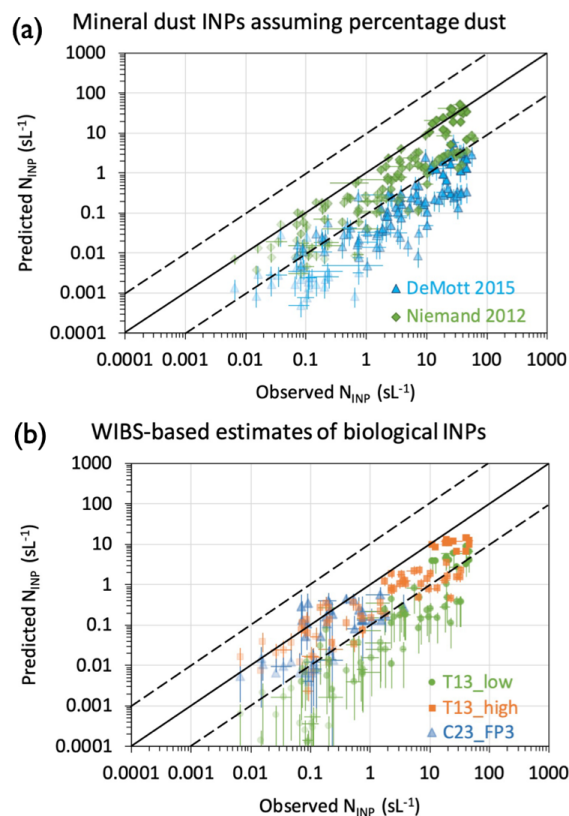
929

930 3) As discussed earlier, we use two definitions of FBAP at sizes larger than 0.5  $\mu\text{m}$  to and  
 931 temperature to predict biological INP concentrations based on Tobo 2013 as defined in  
 932 Section 2.1, presuming to bracket low and high estimates of their links to INPs. We also



933 explore links of higher temperature freezing data ( $> -20$  °C) to FP3 particles, using the  
934 same scalings of the relation between FP3 concentrations and INP concentrations as a  
935 function of temperature that were established by Cornwell et al. (2023) for a coastal  
936 California environment. While we have no reason to expect that these scaling factors  
937 listed in Table 2 are valid for the high altitude, continental environment of FIN-03, they  
938 are starting points to explore this additional link of certain FBAP particles to INPs.

939 To compare these parameterized values with observations, an overall mean observed  
940 immersion freezing  $N_{\text{INP}}$  was calculated for each three-hour period based on all the available data  
941 from all the instruments. This was considered as a reasonable approach since it factors in the  
942 inherent variability found between methods. Immersion freezing  $N_{\text{INP}}$  was predicted for each  
943 parameterization using mean WBS-4A, and LAS data, both at STP concentrations, collected in  
944 the coincident 3-hour periods of time as the INP data. The observed and predicted immersion  
945 freezing  $N_{\text{INP}}$  are plotted against each other in Figure 8. Four temperatures of comparison ( $-15$ ,  $-$   
946  $20$ ,  $-25$  and  $-30$  °C) are presented in Figure 8 for DeMott 2015, Niemand 2012, and Tobo 2013,  
947 while two temperatures of comparison ( $-15$ ,  $-20$  °C) are used for links to FP3-based prediction  
948 of biological INPs. Temperatures are indicated via levels of shading of the data points.  
949 Using the constraint on mineral particles from the combination of PALMS and LAS data for the  
950 campaign average, predicted INPs underestimate the mean INP concentrations at all  
951 temperatures (Figure 8a). The Niemand 2012 surface-area-based INP estimates come modestly  
952 closer to observations, averaging 25% of the total INP concentrations for all times and all  
953 temperatures, while the DeMott 2015 predictions average 4% of INP concentrations, with large  
954 variability apparent. These results can be expected to be highly sensitive to the assessed average



955

956 **Figure 8.** a) Comparison of mean observed  $N_{\text{INP}}$  (all instrument average) and predicted  $N_{\text{INP}}$  calculated  
 957 from DeMott et al. (2015) (DeMott 2015) and Niemand et al. (2012) (Niemand 2012) mineral dust INP  
 958 parameterizations at temperatures  $-30\text{ }^{\circ}\text{C}$ ,  $-25\text{ }^{\circ}\text{C}$ ,  $-20\text{ }^{\circ}\text{C}$ , and  $-15\text{ }^{\circ}\text{C}$  (gradations in shading from dark to  
 959 light) for the PALMS estimated percentages of dust particle number and surface area at sizes above  $0.5$   
 960  $\mu\text{m}$ . Mean  $N_{\text{INP}}$  are averaged over three-hour periods and plotted uncertainties are standard deviations.  
 961 Predicted  $N_{\text{INP}}$  uncertainties are propagated based on 25 % uncertainty in aerosol number and surface area  
 962 concentrations. b) Comparison of mean observed  $N_{\text{INP}}$  and predicted  $N_{\text{INP}}$  calculated from  
 963 parameterizations linking to FBAP concentrations from *Tobo et al.* (2013) (T13\_low and T13\_high; see  
 964 text for description) and from *Cornwell et al.* (2023) (C23\_FP3) following the FP3 particle definition of  
 965 *Wright et al.* (2014). Only  $-15$  and  $-20\text{ }^{\circ}\text{C}$  comparisons are shown for the FP3 prediction. The solid line in  
 966 each plot is the 1:1 line and the dashed lines represent an order of magnitude in both directions.



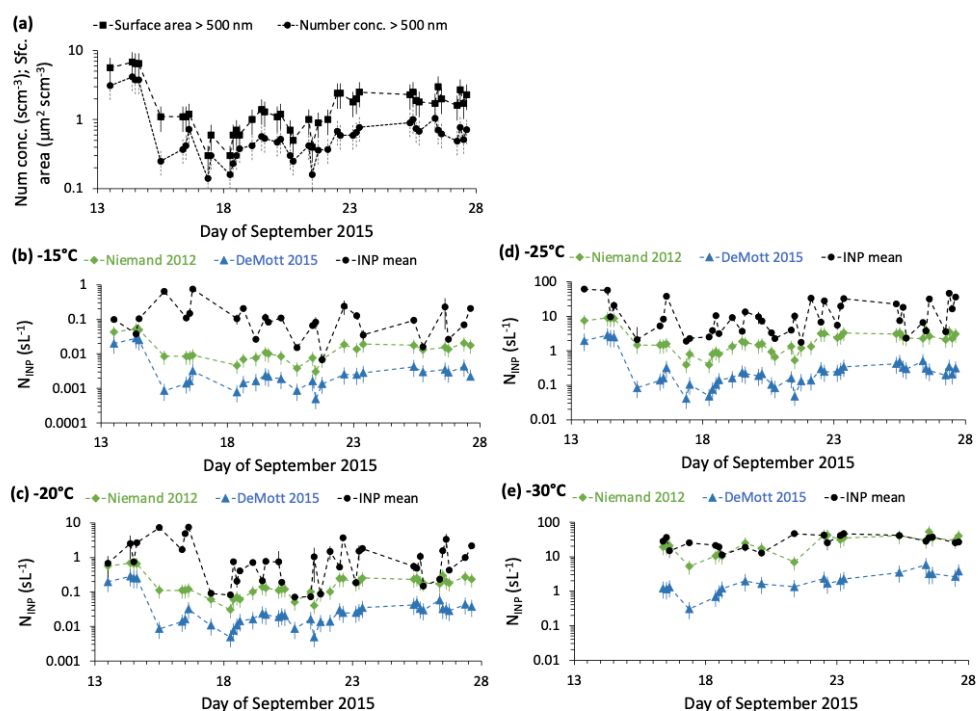


967 mineral particle fraction at sizes above  $0.5 \mu\text{m}$  (varied over the study) and on whether particles  
968 that have a source from regional soils will be represented only by those with mineral content.  
969 Therefore, for comparison, parameterization results using an assumption that all particles at  
970 diameters exceeding  $0.5 \mu\text{m}$  were dust particles are presented in Figure S5. In this case,  
971 admittedly a somewhat unrealistic maximum assumption on mineral dust numbers and surface  
972 area, Niemand 2012 estimates a dust source for 50% and DeMott 2015 estimates 25% of  
973 observed INPs on average. Thus, the predictions of the two parameterizations become more  
974 closely aligned for assumption of more overall mineral dust particles in the size range larger than  
975  $0.5 \mu\text{m}$ . Discrepancy has been noted previously in applying these parameterizations to link to the  
976 aerosol model in an Earth System model for the Southern Ocean region (McCluskey et al.,  
977 2023). In that case, calculations were based on aerosol model derived dust distributions and  
978 occurred under very low dust loading scenarios where neither parameterization has been firmly  
979 tested in the laboratory or field. Under both assumptions on mineral particle number, since  
980 DeMott 2015 was developed based on CFDC measurements for particles  $< 2.5 \mu\text{m}$  in the field  
981 and laboratory, a low bias compared to Niemand 2012 might be expected in comparison to  
982 average immersion freezing data that includes larger particles.

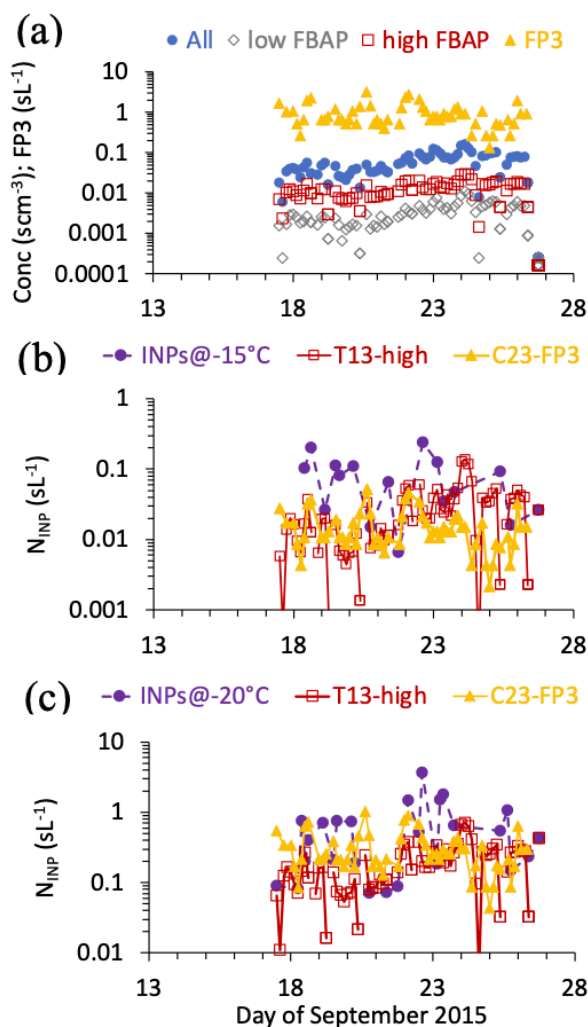
983         The timeline of predicted  $N_{\text{INP}}$  for the two dust parameterizations in comparison to mean  
984 observed  $N_{\text{INP}}$  is shown in Figure 9 for the same temperatures used in Figure 8. These analyses  
985 emphasize that 1) INP observations do not show a special enhancement during the biomass  
986 burning event at the start of FIN-03, and hence closer agreement of the dust parameterizations  
987 with observations at that time is likely an artifact of attributing dust-like INP activation  
988 properties to the dominant biomass burning compositions at that time; 2) the predicted  $N_{\text{INP}}$   
989 trends better with observed  $N_{\text{INP}}$  at temperatures  $< -20 \text{ }^\circ\text{C}$ , as expected for a dominance of dust-



990 like INPs; and 3) the predictions fare less well in describing the observed INP populations at > –  
 991 20 °C where biological INPs may be expected to have greater influence. Thus, these analyses  
 992 overall suggest the presence of a dust-like immersion freezing INP type during FIN-03, but that  
 993 the typical INP efficiency (INP as a function of dust concentration and temperature) attributed to  
 994 mineral dust underestimates the freezing behavior of INPs overall during the period of study.  
 995



996  
 997 **Figure 9.** Time series of aerosol number concentration and surface area (3-h averages at STP) in a), and  
 998 observed mean measured immersion freezing  $N_{\text{INP}}$  (INP mean) plotted with predicted  $N_{\text{INP}}$  from the  
 999 mineral dust parameterizations of Niemand 2012 and DeMott 2015 as described in the main text (all  
 1000 three-hour averages at STP) at temperatures of -15, -20, -25, and -30 °C in b) to e), respectively. Dashed  
 1001 lines are intended only to connect data points and do not imply knowledge of intermediate values.  
 1002 Uncertainties mark one standard deviation above and below the mean values of all parameters.



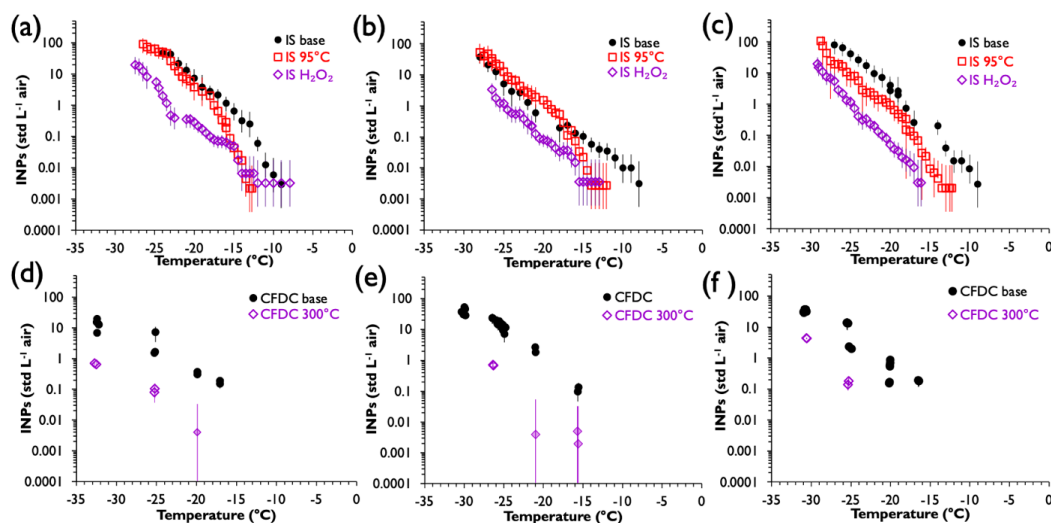
1003

1004 **Figure 10.** a) Timelines of WIBS-based fluorescent particles assignments (all fluorescing in any channel,  
1005 low and high FBAP, and FP3 particles), as defined in the text, during FIN-03. b) INP observed mean  
1006 concentrations and biological INP parameterization predictions linked to high FBAP following Tobo et  
1007 al. (2013) (T13-high) and FP3 particles following Cornwell et al. (2023) at -15 °C in b) and -20 °C in c).

1008



1009 For FIN-03, the Tobo parameterization of biological INPs consistently underpredicted  
1010  $N_{\text{INP}}$ , independent of the WBS FBAP definition used, denoted as T13\_low and T13\_high in  
1011 scatterplot comparison of measured versus predicted values at all times and temperatures in  
1012 Figure 8b and the timeline comparisons at  $-15$  and  $-20$  °C shown in Figure 10. Figure 10 also  
1013 shows the timeline WBS total fluorescent particle concentrations, the high and low FBAP  
1014 concentrations, and FP3 concentrations. The higher FBAP prediction of INPs falls much closer  
1015 to the observations than the low FBAP prediction in Figure 8b and shares some proximal  
1016 equivalence to observations at  $-15$  to  $-20$  °C at times. This result is like that found by Twohy et  
1017 al. (2016) for air over the site where Tobo et al. (2013) collected their data, with the higher  
1018 FBAP estimate bounding the upper end of measured immersion freezing INP concentrations at  
1019 temperatures  $> -20$  °C. Also notable in Figure 8b and Figure 10 is that the C13-FP3 INP  
1020 concentration predictions filled a similar space as the T13\_high estimates, coming closest  
1021 together at  $-20$  °C. While these results suggest that biological INP parameterizations can explain  
1022 the higher temperature INP concentrations observed during FIN-03, with caveats on the large  
1023 and likely not fully quantifiable uncertainty in such predictions, the temporal analysis  
1024 (Figure S6) indicates that there is no consistent temporal agreement between predicted and  
1025 measured INPs, even if different scaling factors were applied to the predictions. Predictions at  
1026  $-20$  °C again show the best overall agreement, while those at  $-15$  °C suggest that the Cornwell et  
1027 al. (2023) scaling factor should be higher for the SPL site at the time of FIN-03 to better describe  
1028 mean values of biological INP concentrations using the FP3 particle signal.  
1029



1030

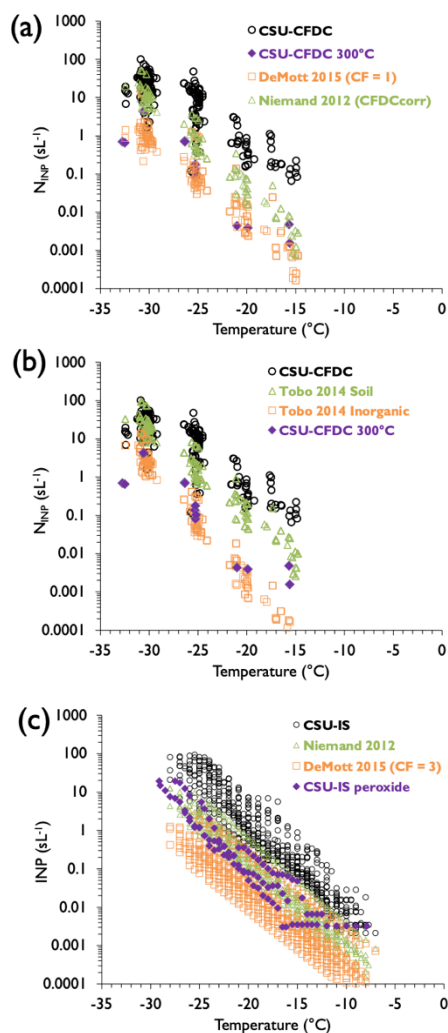
1031 **Figure 11.** Summary of treated IS filter suspensions using heat and peroxide (a, b, c) and dry heat-treated  
 1032 CSU CFDC single particle data (d, e, f), for September 15, 23 and 25 (a-c, d-f, respectively). Error bars  
 1033 represent 95% confidence intervals for individual experimental spectra for the CSU-IS and for individual  
 1034 CSU CFDC measurements.

1035 The results of CSU-IS and CSU-CFDC treatments on INP concentrations measured for  
 1036 three (of 21 overall) intercomparison time periods are shown in Figure 11, for examination of  
 1037 consistency with the results of the diagnostic parameterization analysis just discussed. In Figure  
 1038 11a-c, it is seen that thermal treatments indicated the strong contribution of inferred biological  
 1039 INPs primarily at temperatures higher than about  $-20^{\circ}\text{C}$ , but that peroxide digestion of organic  
 1040 compounds lowered INP activity at all tested temperatures by an order of magnitude on average.  
 1041 Similar reductions of INPs measured for single particles by the CSU-CFDC following dry  
 1042 heating (Figure 11d-e) demonstrate strong consistency with the IS results for bulk immersion  
 1043 freezing on the dominance of organic INP compositions, even though CSU-CFDC measured  
 1044 unamended INP concentrations were always lower. The CSU-IS heat treatment results (Figure



1045 11a-c) suggest that biological INPs may have been ubiquitous during FIN-03 at temperatures  
1046 above  $-20^{\circ}\text{C}$ , and extended to lower temperatures at times, as indicated by the results from  
1047 September 25. This is broadly consistent with the parameterization results based on FBAP  
1048 measurements, although the Tobo 2013 and FP3 parameterizations did not capture all the  
1049 influence of apparent biological INPs during the study. Whether for size-limited ( $< 2.5\ \mu\text{m}$ ) as in  
1050 CSU-CFDC measurements, or bulk aerosol collected for CSU-IS immersion freezing  
1051 measurements, the inferred INP compositions typically dominated by organics at temperatures  $<$   
1052  $-20^{\circ}\text{C}$  could reflect origins from arable soil dusts (Testa et al., 2021) that surround the region of  
1053 study. Biomass burning aerosols also have influence as organic INPs (Schill et al, 2020; Barry et  
1054 al., 2021). However, while biomass burning type particles were noted as a prevalent composition  
1055 in FIN-03, these types of potential INPs likely cannot explain INP concentrations in FIN-03  
1056 because Barry et al. (2021) showed that Western U.S. biomass burning INPs have active site  
1057 densities about 3 orders of magnitude lower than those attributed to dust particles that also were  
1058 ubiquitous at modest number concentrations during FIN-03. Furthermore, the strong biomass  
1059 burning event noted on September 14 had only modest, if any, apparent impacts on INP  
1060 concentrations despite greatly elevated aerosol concentrations and surface areas, as already  
1061 mentioned above (Figure 9).

1062 Finally, in Figure 12 we address whether the treatment results support the conclusion of  
1063 the diagnostic parameterization analysis suggesting that inorganic INPs (mineral particles in  
1064 particular) were of minor influence during FIN-03. We introduce the additional parameterization  
1065 of Tobo et al. (2014) (Tobo 2014) for arable soil dust INPs as part of this discussion. Tobo et al.  
1066 (2014) parameterized the ice nucleation behavior of soil dusts from Wyoming, regionally  
1067 proximal to the FIN-03 site at SPL, specifically using the CSU CFDC and the dry heat method at



1068

1069 **Figure 12.** a) Comparison of all untreated CSU CFDC data (black circles), cases after passing through the  
 1070 upstream 300 °C tube heater (purple diamonds), and calculations from the DeMott 2015 dust  
 1071 parameterization in (orange squares) and with CF = 1 as appropriate for a direct comparison to CSU  
 1072 CFDC data (see text). b) The same exercise as in a) but using predictions of total soil organic INP  
 1073 concentrations and inorganic INP concentrations within soil INPs, both from Tobo et al. (2014). c) The  
 1074 same exercise but for all CSU-IS data and the cases with peroxide digestion. In this case, CF = 3 must be  
 1075 used in DeMott 2015 and the mineral dust INP prediction of Niemand 2012 is also shown.



1076 300 °C to indicate organic versus inorganic INP contributions from such soil particles. This  
1077 parameterization, like Niemand 2012, is based on the surface area of dust particles and so we  
1078 apply the same assumptions as before to restrict to the proportion of dust larger than 0.5 µm.  
1079 Since the CSU-CFDC is also restricted to measuring INPs at diameters below 2.5 µm, we apply  
1080 a correction factor to the surface area to account for the fact that the surface area at below this  
1081 size was 90% of the project average total surface area. No significant impact of the treatments is  
1082 assumed on aerosol concentrations or surface area at sizes above 0.5 µm in Figure 12.

1083         Figures 12a and 12b focus on specific comparisons to CSU-CFDC data. In Figure 12a, it  
1084 is seen that INP concentrations predicted by the DeMott 2015 parameterization for sampling  
1085 periods during the entire campaign show remarkable agreement with the 300 °C CSU-CFDC  
1086 data on selected days when applying  $CF = 1$  in the parameterization, as is appropriate for a direct  
1087 comparison to instrument data that is uncorrected for the underestimates that led to selecting  $CF$   
1088  $= 3$  for modeling studies. In Figure 12 b, it is shown that the Tobo 2014 parameterizations for  
1089 untreated soil dusts and the inorganic remnants also give very good agreement with CFDC  
1090 untreated and treated data, supporting the likely important influence of such arable soil dusts  
1091 during FIN-03. Predictions for untreated soils do not quite reach the level of the observed INPs,  
1092 but this could be explained by the additional contribution of biological INPs that has already  
1093 been discussed.

1094         In Figure 12c, direct comparisons of the Niemand 2012 and DeMott 2015 predictions for  
1095 mineral dust INPs for the entire project are shown in comparison to the CSU-IS untreated and  
1096 H<sub>2</sub>O<sub>2</sub> treated data on selected days. The DeMott 2015 prediction of INP concentrations uses  $CF$   
1097  $= 3$  in this case, as appropriate. The same discrepancy between the DeMott 2015 and Niemand  
1098 2012 predictions as discussed already regarding Figure 8a appears in this comparison.

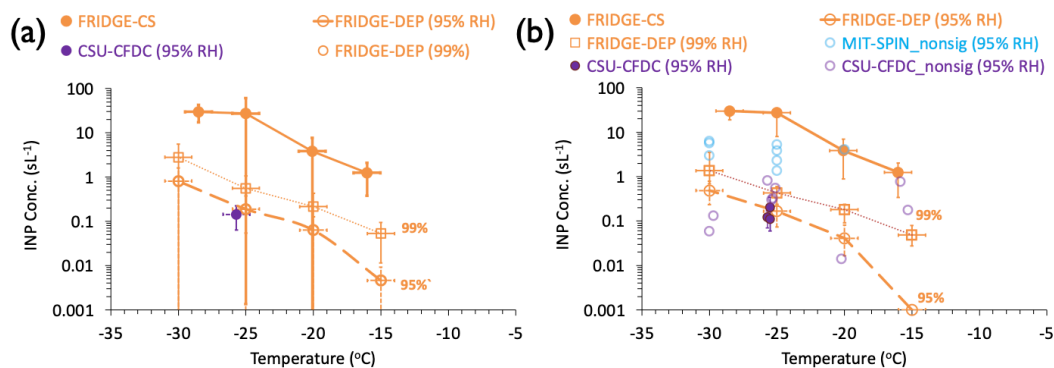




1099 Nevertheless, it is seen that both parameterizations grossly underestimate untreated CSU-IS INP  
1100 concentrations and the treated CSU-IS results fall between the predicted values, agreeing better  
1101 with the Niemand 2012 parameterization. While one might wish to allude to the fact that the IS  
1102 filters sample particle sizes, to 10  $\mu\text{m}$  and possible larger that may have higher ice nucleation  
1103 efficiencies, while the CSU-CFDC was restricted to sampling particles  $<2.5 \mu\text{m}$  as a source for  
1104 the lower DeMott 2015 estimate in comparison to CSU-IS data, we have already addressed that  
1105 there was no general consistency in INP concentrations for methods that sampled similar size  
1106 particles overall. The best that can be stated is that the parameterization exercises and treatment  
1107 data strongly support that inorganic INPs were of weak influence during FIN-03 and that arable  
1108 soil dusts and biological INPs accounted for the strongest influences during sampling, akin to the  
1109 findings of Testa et al. (2021).

### 1110 **3.6 Observations of INPs in the deposition nucleation regime**

1111 Measurements of deposition nucleation  $N_{\text{INP}}$  are summarized in Figures 13 and 14.  
1112 FRIDGE-DEP nucleation substrates were collected for 1 to 5 periods on many days during  
1113 FIN-03 and processed at 5-degree interval temperatures from  $-15$  to  $-30$   $^{\circ}\text{C}$ , and for setpoint  
1114 humidity of 95% and 99% RH (uncertainties to 2%). Data collected at 102% via the standard  
1115 FRIDGE methods are not included herein. CSU-CFDC and MIT-SPIN deposition data were  
1116 collected nominally at 95% RH with an uncertainty of about 2.5% RH, and at a range of  
1117 temperatures on different days. Mean values and standard deviation error bars of the FRIDGE-  
1118 DEP data are shown in Figure 13a and median values of FRIDGE-DEP  $N_{\text{INP}}$  (with interquartile  
1119 values as error bars) are shown in Figure 13b. Standard deviations were large over the course of  
1120 the study for comprehensive FRIDGE-DEP data when binned at 5-degree interval temperatures.  
1121 Nevertheless, average concentrations of deposition INPs measured by the FRIDGE-DEP

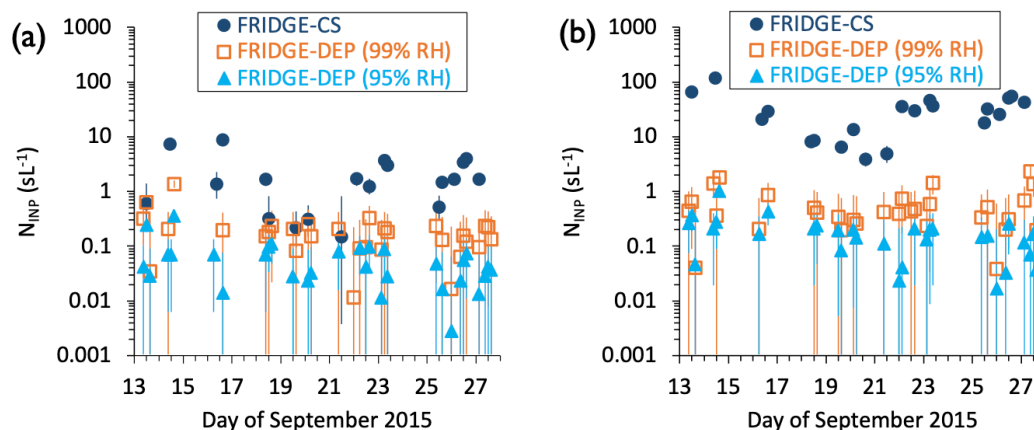


1122

1123 **Figure 13.** Summary of deposition-mode  $N_{\text{INP}}$  ( $\text{sL}^{-1}$ ) as a function of temperature. In a), mean FRIDGE-  
 1124 DEP data at 95% (open orange circles) and 99% (open orange squares) RH are shown along with mean  
 1125 immersion freezing data from the FRIDGE-CS (filled orange circles) and the mean for the few cases of  
 1126 statistically significant CSU-CFDC data (filled purple circle) at 95% RH. Error bars are one standard  
 1127 deviation of the means. In b), median FRIDGE-DEP data are shown and error bars for these are the 95%  
 1128 confidence intervals. The significant CSU-CFDC measurement points at 95% RH are also shown with  
 1129 their 95% confidence intervals. Data measured at 95% RH from the CSU-CFDC and MIT-SPIN that were  
 1130 positively valued but failed significance testing are shown without errors as open purple and open blue  
 1131 circles, respectively.

1132

1133 indicated a consistent 3-5 factor increase between 95 and 99% RH over the range of  
 1134 temperatures investigated.  $N_{\text{INP}}$  concentration differences at the two RH values were slightly  
 1135 smaller for median values (Figure 13b), and the median values are slightly lower than the means.  
 1136 Finally, FRIDGE-CS values are plotted in each panel of Figure 13, indicating that FRIDGE-DEP  
 1137  $N_{\text{INP}}$  concentrations averaged for 99% RH are factors 10 to 30 lower than average immersion  
 1138 freezing  $N_{\text{INP}}$  concentrations, depending on temperature.



1139

1140 **Figure 14.** Time series of FRIDGE-CS (immersion freezing) and FRIDGE-DEP (deposition)  $N_{INP}$   
 1141 measured at a)  $-20\text{ }^{\circ}\text{C}$ , and b)  $-25\text{ }^{\circ}\text{C}$ . Data are from individual filters or wafer collections and error bars  
 1142 are 95% confidence intervals.

1143 One day of significant data was obtained for the CSU-CFDC deposition measurements  
 1144 while using the aerosol concentrator, on September 14, containing three different time periods.  
 1145 These are averaged to create the only online data point represented as a mean in Figure 13a. The  
 1146 individual period measurements from this day, with confidence intervals as errors, are shown for  
 1147 the CSU-CFDC in Figure 13b. Thereby it is seen that these measurements at close to  $-25\text{ }^{\circ}\text{C}$   
 1148 agree very well with the mean FRIDGE deposition  $N_{INP}$  at  $-25\text{ }^{\circ}\text{C}$  and 95% RH. No  
 1149 measurements of significance were achieved with the MIT-SPIN when operating in the  
 1150 deposition regime. In fact, the most common CSU-CFDC and MIT-SPIN deposition nucleation  
 1151  $N_{INP}$  results were below instrument detection limits, not meeting the test for significance, as  
 1152 shown for all periods from 6 common days of such observations represented in Figure 13b.  
 1153 Understanding that these data represent a failure to collect statistically-defensible data, the non-  
 1154 significant data generally scatter about the significant CSU-CFDC data and the FRIDGE-DEP



1155 data at 95% RH, with a higher bias for the MIT-SPIN data. This indicates the difficulty for  
1156 online continuous flow instruments to capture low deposition  $N_{\text{INP}}$  concentration data that fall  
1157 below  $1 \text{ sL}^{-1}$  at most times, considering the FRIDGE-DEP data as the standard. Higher sample  
1158 volumes and limited background frost conditions are needed to sense these low atmospheric INP  
1159 concentrations.

1160 Time series of the FRIDGE-DEP measurements at  $-20 \text{ }^{\circ}\text{C}$  and  $-25 \text{ }^{\circ}\text{C}$  are shown in  
1161 Figure 14. Deposition-mode  $N_{\text{INP}}$  has been averaged over three-hour periods for this analysis.  
1162 The FRIDGE immersion freezing data is included in this figure to allow for direct comparison  
1163 temporally. Immersion freezing  $N_{\text{INP}}$  generally exceeded deposition-mode  $N_{\text{INP}}$  when both types  
1164 of measurements were collected by the two FRIDGE operational methods within the same period  
1165 (or during adjacent time periods). This difference ranged from 0 to 2 orders of magnitude, with  
1166 the largest differences seen at  $-25 \text{ }^{\circ}\text{C}$  and a period of insignificant differences between the mode  
1167 results seen only from the 18<sup>th</sup> to the 22<sup>nd</sup> of September at  $-20 \text{ }^{\circ}\text{C}$  (Figure 14a).

1168 Based on these FRIDGE-CS and FRIDGE-DEP results, immersion-mode ice nucleation  
1169 dominates at most times at mixed-phase cloud temperatures. Nevertheless, deposition-mode ice  
1170 nucleation contributes modestly to the pool of INP at mixed-phase cloud temperatures in the  
1171 atmosphere, and thus may bear consideration for parameterization in atmospheric models. The  
1172 ability of online ice nucleation instruments to measure  $N_{\text{INP}}$  in the deposition mode in  
1173 correspondence to offline measurements has not been confirmed due to the mentioned inability  
1174 of the online instruments used in FIN-03 to capture the low deposition nucleation  $N_{\text{INP}}$   
1175 concentrations. More work should be carried out on measurements of INPs in the deposition  
1176 mode to understand variabilities in time and their relation to INP size and composition, as well as  
1177 to resolve if online measurements can be improved. For the time being, the substrate methods



1178 appear to be recommended for ambient atmospheric measurements in the realm below water  
1179 saturation at mixed-phase cloud temperatures.

1180

#### 1181 **4. Summary and conclusions**

1182 FIN-03 was an ice nucleation instrument intercomparison conducted in the challenging  
1183 environment of the high-altitude mountaintop field setting. Two online systems (CSU-CFDC,  
1184 MIT-SPIN) and three offline systems (FRIDGE, CSU-IS, NC State-CS) were represented in  
1185 FIN-03. The immersion freezing INP concentrations measured in FIN-03 spanned a dynamic  
1186 range of over five orders of magnitude ( $10^{-3}$  to  $\sim 10^2$  L<sup>-1</sup>) over the temperature range  $-35$  °C to  $-5$   
1187 °C. Agreement within one order of magnitude in immersion freezing  $N_{\text{INP}}$  was generally  
1188 observed between all ice nucleation instruments measuring immersion INP concentrations at any  
1189 given temperature if measurement and sampling times were matched to within 3 hours. Better  
1190 than one order of magnitude agreement was found at temperatures lower than  $-25$  °C and higher  
1191 than  $-18$  °C, with occasional deviations larger than an order of magnitude in the temperature  
1192 range  $-25$  °C to  $-18$  °C. We do not have a full understanding of what controls better or worse  
1193 agreement at different times or different temperatures, though some factors have been previously  
1194 discussed in documenting FIN-02 laboratory studies (DeMott et al., 2018). In this study, there  
1195 was some inference that the different filters and impinger used did not equally capture particles  
1196 in all size ranges, which is something to improve on in future studies. Given the constant changes  
1197 in the concentration, size distribution and composition of the ambient aerosol population,  
1198 inevitable with any field campaign, this level of agreement represents state-of-the-art, at least as  
1199 judged based on recent laboratory and other field comparisons using similar instrumentation  
1200 (e.g., Knopf et al., 2021; Lacher et al., 2024).



1201            Although FIN-03 was not conducted as a closure study per se, ancillary data on aerosol  
1202 sizes and compositions as recommended in more recent discussions of needs for true closure  
1203 exercises (Knopf et al., 2021; Burrows et al., 2022) were purposefully collected for integration  
1204 into analyses. This included explicit measurements of the aerosol size distribution, and single  
1205 particle measurements of aerosol chemical and biological composition. These measurements  
1206 allowed inferences to be made about INP compositions that provide context for the period of  
1207 study and establish an example for future intercomparison and long-term measurement efforts.  
1208 Through comparing INP data to some current parameterizations describing biological, mineral  
1209 and soil dust INPs, and additional direct investigations of INP composition via certain pre-  
1210 treatments to remove biological and organic immersion-freezing INPs, these investigations  
1211 revealed ubiquitous biological and organic-influenced soil-dust-like INP influences that mimic  
1212 those found over other continental regions (Knopf et al., 2021; Testa et al., 2021; Lacher et al.,  
1213 2024). Biological INPs were indicated via selected immersion freezing heat treatments to be  
1214 dominant at  $> -20$  °C, although of potential influence at all mixed-phase temperatures.  
1215 Prediction of these based on parameterizations that utilize single particle fluorescence data (Tobo  
1216 et al., 2013; Wright et al., 2014; Cornwell et al., 2023) suggest the average utility of such  
1217 parameterizations but these were unable to predict the full temporal variation of biological INPs.  
1218 This suggests that local variations of these INPs, which may in fact represent multiple biological  
1219 particle types, is an area that requires more effort. Based on relatively good consistency between  
1220 predicted and measured mineral influences on immersion-freezing  $N_{\text{INP}}$  concentrations, strictly  
1221 mineral or other inorganic components of INPs were suggested to have a modest contribution to  
1222 total INP concentrations at most times and at the freezing temperatures probed during this study.  
1223 As in most prior studies, the mineral influence became stronger at the lowest temperatures



1224 assessed. In contrast, it was found by comparison to a parameterization based on proximally  
1225 regional soil particles that arable soil INPs likely explained the second most important  
1226 contribution of INPs during FIN-03, those emanating from other organic particle components  
1227 that may have been internally mixed with minerals. Biomass burning influences were possible  
1228 but appear to have not contributed greatly to the climatology of INPs during the study. It was  
1229 critically important in arriving at these conclusions to have single particle aerosol composition  
1230 data, from a mass spectrometer that could discern the sizes and fractional contribution of  
1231 minerals and from a laser-based single particle fluorescence measurement to estimate the  
1232 biological character of particles. Nevertheless, a great amount of work is still needed to generally  
1233 parameterize the mixed INP populations that may occur temporally in the atmosphere at higher  
1234 altitude sites like SPL, or anywhere for that matter.

1235         Importantly, FIN-03 included an assessment of the separate relative contributions of  
1236 deposition and immersion freezing INP concentrations, one of the few existing data sets of this  
1237 kind. The offline FRIDGE-DEP method was used to acquire comprehensive deposition  $N_{\text{INP}}$   
1238 measurements in dependence on RH (95 and 99%), while the CSU-CFDC and MIT-SPIN  
1239 instruments attempted focused deposition nucleation measurements at (nominally) 95% RH on  
1240 several days. As expected, FRIDGE-DEP measurements indicated factor of a few increases in  
1241 deposition  $N_{\text{INP}}$  concentrations between 95 to 99% RH. Also, deposition  $N_{\text{INP}}$  concentrations  
1242 were nearly always lower than immersion freezing  $N_{\text{INP}}$  concentrations. Deposition INP  
1243 concentrations at most times at 99% RH (always at 95% RH) were lower by an order of  
1244 magnitude than immersion freezing INP concentrations at  $-20\text{ }^{\circ}\text{C}$  and by more than an order of  
1245 magnitude at  $-25\text{ }^{\circ}\text{C}$ . For the online instruments, only limited periods of deposition INP  
1246 measurements on one day achieved statistical significance from the CSU-CFDC data. While



1247 these data were in good agreement with FRIDGE-DEP data at  $-25^{\circ}\text{C}$  and 95% RH, the most  
1248 striking result was that all other measurement periods for the CSU-CFDC and MIT-SPIN gave  
1249 measurements that were not significant at the 95% confidence level. Thus, currently, offline  
1250 methods for measuring deposition INPs appear to offer the best chance for success in measuring  
1251 the lower concentrations of INPs that activate below water saturation in the mixed-phase  
1252 temperature regime. It would be useful to make such assessments at a variety of sites to confirm  
1253 measurements made during FIN-03 on the relative contributions and variability of INPs active in  
1254 these conditions toward ice formation in clouds. Additional instrument developments for online  
1255 measurements of these, and future intercomparisons, will be useful.

1256 In summary, the relative agreements amongst instruments during FIN-03 that match those  
1257 found in the FIN-02 laboratory studies are encouraging and represent steady improvement in the  
1258 community's collective ability to detect and quantify atmospheric ice nucleation. There was not a  
1259 clear divide between the ability of online and offline systems to measure INP concentrations  
1260 from the data collected in this study, although the need to carefully consider aerosol sampling  
1261 efficiencies for different instruments was highlighted as a potential issue in this study, and one  
1262 requiring close attention in future studies. In principle, both types of instruments show excellent  
1263 promise for future field studies. For full closure studies of ice nucleation by atmospheric  
1264 aerosols, methods for identifying INP composition as demonstrated herein and recommended by  
1265 other recent discussions in Knopf et al. (2021) and Burrows et al. (2022) are critical for  
1266 understanding and improving INP measurements overall.

1267





1268 **Data availability** All data used for the figures in this paper can be accessed at

1269 <https://radar.kit.edu/radar/en/dataset/eGhfvcOhsOyADZXXN> (persistent

1270 doi:10.35097/eGhfvcOhsOyADZXXN)

1271 **Author contributions**

1272 Paul J. DeMott, Jessica A. Mirrielees and Sarah D. Brooks wrote the paper with assistance from  
1273 all teams and authors contributing information on instrument descriptions and comments on all  
1274 results and conclusions, with contributions from Jake Zenker on some data analysis. Paul J.  
1275 DeMott, Ezra J.T. Levin, Thea Schiebel, Kaitlyn Suski, and Tom Hill provided data and analyses  
1276 from the CSU-CFDC and IS instruments. Daniel J. Cziczo, Martin J. Wolfe, Sarvesh Garimella,  
1277 and Maria Zawadowicz provided MIT-SPIN team measurements and analyses. Markus D.  
1278 Petters and Sarah S. Petters provided data and analysis for the NC State-CS instrument. Heinz G.  
1279 Bingemer, Jann Schrod, and Daniel Weber provided data and analyses for the FRIDGE  
1280 instrument. Anne Perring provided data and analyses for the WIBS-4A. Karl Froyd provided  
1281 data and analyses for the LAS and PALMS. Anna Gannet Hallar and Ian McCubbin oversaw  
1282 field operations, coordinated with visiting teams at Storm Peak Laboratory, and provided  
1283 nephelometer and meteorological measurements. Paul J. DeMott, Daniel J. Cziczo, Ottmar  
1284 Möhler contributed to organize the campaign in connection with the other FIN activities.

1285

1286 **Competing interests**

1287 The contact author has declared that none of the authors has any competing interests.

1288 **Acknowledgements**



1289 Partial financial support for this project was provided by the U.S. National Science  
1290 Foundation, Grant No. AGS-1339264 and U.S. Department of Energy's Atmospheric System  
1291 Research, an Office of Science, Office of Biological and Environmental Research program,  
1292 under grant no. DE-SC0014487. Paul J. DeMott, Ezra J.T. Levin, Thea Schiebel, Kaitlyn Suski,  
1293 and Tom Hill acknowledge partial and in-kind research support during FIN-03 from NSF grant  
1294 no. AGS-1358495. Markus Petters acknowledges partial and in-kind support during FIN-03 from  
1295 NSF grant no. AGS-1450690. Jann Schrod acknowledges research support from the European  
1296 Union's Seventh Framework Programme (FP7/2007-2013) project BACCHUS under grant  
1297 agreement no. 603445. Heinz G. Bingemer and Daniel Weber acknowledge research support  
1298 under DFG grant BI 462/3-2. Thea Schiebel and Ottmar Möhler received support through the  
1299 German Science Foundation Projects INUIT and INUIT-2 (MO 668/4-1 and MO 668/4-2). Anne  
1300 Perring acknowledges support from the NOAA Health of the Atmosphere Program and the  
1301 NOAA Atmospheric Composition and Climate Program. Special thanks to Romy Fösig (Ullrich)  
1302 for assistance with data archival.

1303

1304



## 1305 References

- 1306 Alsante, A. N., Thornton, D. C. O., & Brooks, S. D.: Ice nucleation catalyzed by the  
1307 photosynthesis enzyme RuBisCO and other abundant biomolecules. *Communications*  
1308 *Earth & Environment*, 4(1). doi:10.1038/s43247-023-00707-7, 2023.
- 1309 Agresti, A. and Coull, B. A.: Approximate is better than "exact" for interval estimation of  
1310 binomial proportions, *The American Statistician*, 52, 119-126,  
1311 <https://doi.org/10.1080/00031305.1998.10480550>, 1998.
- 1312 Andreae, M. O., & Rosenfeld, D.: Aerosol-cloud-precipitation interactions. Part 1. The nature  
1313 and sources of cloud-active aerosols. *Earth-Science Reviews*, 89(1-2), 13-41.  
1314 <https://doi.org/10.1016/j.earscirev.2008.03.001>, 2008.
- 1315 Andrews, E., and Coauthors, 2019: Overview of the NOAA/ESRL Federated Aerosol  
1316 Network. *Bull. Amer. Meteor. Soc.*, **100**, 123–135, <https://doi.org/10.1175/BAMS-D-17-0175.1>.
- 1317  
1318 Ardon-Dryer, K., & Levin, Z.: Ground-based measurements of immersion freezing in the eastern  
1319 Mediterranean. *Atmospheric Chemistry and Physics*, 14(10), 5217-5231.  
1320 <https://doi.org/10.5194/acp-14-5217-2014>, 2014.
- 1321 Barry, K. R., Hill, T. C. J., Levin, E. J. T., Twohy, C. H., Moore, K. A., Weller, Z. D., Toohey, D. W., Reeves,  
1322 M., Campos, T., Geiss, R., Fischer, E. V., Kreidenweis, S. M., and DeMott, P. J.: Observations of ice  
1323 nucleating particles in the free troposphere from western US wildfires. *Journal of Geophysical*  
1324 *Research: Atmospheres*, **126**, e2020JD033752. <https://doi.org/10.1029/2020JD033752>, 2021.
- 1325 Barry, K. R., Hill, T. C. J., Jentsch, C., Moffett, B. E., Stratmann, F., and DeMott, P.J.: Pragmatic protocols  
1326 for working cleanly when measuring ice nucleating particles, *Atmospheric Research*, **250**, 105419,  
1327 <https://doi.org/10.1016/j.atmosres.2020.105419>, 2021
- 1328 Beall, C. M., Lucero, D., Hill, T. C. J., DeMott, P. J., Stokes, M. D., and Prather, K. A.: Best  
1329 practices for precipitation sample storage for offline studies of ice nucleation in marine  
1330 and coastal environments, *Atmos. Meas. Tech.*, 13, 6473–6486,  
1331 <https://doi.org/10.5194/amt-13-6473-2020>, 2020
- 1332 Boose, Y., Sierau, B., Isabel García, M., Rodríguez, S., Alastuey, A., Linke, C., Schnaiter, M.,  
1333 Kupiszewski, P., Kanji, Z. A., and Lohmann, U.: Ice nucleating particles in the Saharan  
1334 Air Layer. *Atmospheric Chemistry and Physics*, 16(14), 9067-9087.  
1335 <https://doi.org/10.5194/acp-16-9067-2016>, 2016.
- 1336 Boucher, O., Randall, D., Artaxo, P., Bretherton, C., Feingold, G., Forster, P., Kerminen, V.-M.,  
1337 Kondo, Y., Liao, H., Lohmann, U., Rasch, P., Satheesh, S. K., Sherwood, S., Stevens, B.,  
1338 and Zhang, X. Y.: *Clouds and Aerosols. In: Climate Change 2013: The Physical Science*  
1339 *Basis. Contribution of Working Group I to the Fifth Assessment Report of the*  
1340 *Intergovernmental Panel on Climate Change*. Retrieved from Cambridge, United  
1341 Kingdom and New York, NY, USA, 2013.
- 1342 Collaud Coen, M., Andrews, E., Aliaga, D., Andrade, M., Angelov, H., Bukowiecki, N., Ealo,  
1343 M., Fialho, P., Flentje, H., Hallar, A. G., Hooda, R., Kalapov, I., Krejci, R., Lin, N.-H.,  
1344 Marinoni, A., Ming, J., Nguyen, N. A., Pandolfi, M., Pont, V., Ries, L., Rodríguez, S.,  
1345 Schauer, G., Sellegri, K., Sharma, S., Sun, J., Tunved, P., Velasquez, P., and Ruffieux,  
1346 D.: Identification of topographic features influencing aerosol observations at high altitude  
1347 stations: Identification of topographic features influencing aerosol observations at high



- 1348 altitude stations. *Atmospheric Chemistry and Physics*, 18(16), 12289-12313.  
1349 <https://doi.org/10.5194/acp-18-12289-2018>, 2018.
- 1350 Coluzza, I., Creamean, J., Rossi, M. J., Wex, H., Alpert, P. A., Bianco, V., Boose, Y., Dellago,  
1351 C., Felgitsch, L., Fröhlich-Nowoisky, J., Herrmann, H., Jungblut, S., Kanji, Z. A., Menzl,  
1352 G., Moffett, B., Moritz, C., Mutzel, A., Pöschl, U., Schauer, M., Scheel, J., Stopelli, E.,  
1353 Stratmann, F., Grothe, H., and Schmale, D. G.: Perspectives on the Future of Ice  
1354 Nucleation Research: Research Needs and Unanswered Questions Identified from Two  
1355 International Workshops. *Atmosphere*, 8(8). <https://doi.org/10.3390/atmos8080138>, 2017.
- 1356 Cornwell, G. C., McCluskey, C. S., Hill, T. C. J., Levin, E. J. T., Rothfuss, N. E., Taia, S.-L.,  
1357 Petters, M. D., DeMott, P. J., Martin, A., Kreidenweis, S. M., Prather, K. A. and  
1358 Burrows, S. M.: Bioaerosols are the dominant source of warm-temperature immersion-  
1359 mode INPs and drive uncertainties in INP predictability in the ambient atmosphere.  
1360 *Science Advances*, 9, eadg3715, <https://doi.org/10.1126/sciadv.adg3715>, 2023.
- 1361 Cornwell, G. C., McCluskey, C. S., Levin, E. J. T., Suski, K. J., DeMott, P. J., Kreidenweis, S.  
1362 M., & Prather, K. A.: Direct online mass spectrometry measurements of ice nucleating  
1363 particles at a California coastal site. *Journal of Geophysical Research: Atmospheres*, 124,  
1364 12,157–12,172. <https://doi.org/10.1029/2019JD030466>, 2019.
- 1365 Creamean, J. M., Suski, K. J., Rosenfeld, D., Cazorla, A., DeMott, P. J., Sullivan, R. C., White,  
1366 A. B., Ralph, F. M., Minnis, P., Comstock, J. M., Tomlinson, J. M., and Prather, K. A.:  
1367 Dust and biological aerosols from the Sahara and Asia influence precipitation in the  
1368 western U.S. *Science*, 339(6127), 1572-1578. <https://doi.org/10.1126/science.1227279>,  
1369 2013.
- 1370 David, R. O., Fahrni, J., Marcolli, C., Mahrt, F., Brühwiler, D., and Kanji, Z. A: The role of  
1371 contact angle and pore width on pore condensation and freezing, *Atmos. Chem. Phys.*, 20,  
1372 9419–9440, <https://doi.org/10.5194/acp-20-9419-2020>, 2020.
- 1373 David, R. O., Cascajo-Castresana, M., Brennan, K. P., Rösch, M., Els, N., Werz, J., Weichlinger,  
1374 V., Boynton, L. S., Bogler, S., Borduas-Dedekind, N., Marcolli, C., and Kanji, Z. A.:  
1375 Development of the DRoplet Ice Nuclei Counter Zurich (DRINCZ): validation and  
1376 application to field-collected snow samples, *Atmos. Meas. Tech.*, 12, 6865–6888,  
1377 <https://doi.org/10.5194/amt-12-6865-2019>, 2019.
- 1378 DeMott, P. J., Mohler, O., Cziczo, D. J., Hiranuma, N., Petters, M. D., Petters, S. S., Belosi, F.,  
1379 Bingemer, H. G., Brooks, S. D., Budke, C., Burkert-Kohn, M., Collier, K. N.,  
1380 Danielczok, A., Eppers, O., Felgitsch, L., Garimella, S., Grothe, H., Herenz, P., Hill, T.  
1381 C. J., Höhler, K., Kanji, Z. A., Kiselev, A., Koop, T., Kristensen, T. B., Krüger, K.,  
1382 Kulkarni, G., Levin, E. J. T., Murray, B. J., Nicosia, A., O'Sullivan, D., Peckhaus, A.,  
1383 Polen, M. J., Price, H. C., Reicher, N., Rothenberg, D. A., Rudich, Y., Santachiara, G.,  
1384 Schiebel, T., Schrod, J., Seifried, T. M., Stratmann, F., Sullivan, R. C., Suski, K. J.,  
1385 Szakáll, M., Taylor, H. P., Ullrich, R., Vergara-Temprado, J., Wagner, R., Whale, T. F.,  
1386 Weber, D., Welti, A., Wilson, T. W., Wolf, M. J., Zenker, J.: The Fifth International  
1387 Workshop on Ice Nucleation phase 2 (FIN-02): laboratory intercomparison of ice  
1388 nucleation measurements. *Atmospheric Measurement Techniques*, 11(11), 6231-6257.  
1389 <https://doi.org/10.5194/amt-11-6231-2018>, 2018.
- 1390 DeMott, P. J., Hill, T. C. J., Petters, M. D., Bertram, A. K., Tobo, Y., Mason, R. H., Suski, K. J.,  
1391 McCluskey, C. S., Levin, E. J. T., Schill, G. P., Boose, Y., Rauker, A. M., Miller, A. J.,  
1392 Zaragoza, J., Rocci, K., Rothfuss, N. E., Taylor, H. P., Hader, J. D., Chou, C., Huffman,  
1393 J. A., Pöschl, U., Prenni, A. J., and Kreidenweis, S. M.: Comparative measurements of



1394 ambient atmospheric concentrations of ice nucleating particles using multiple immersion  
1395 freezing methods and a continuous flow diffusion chamber, *Atmos. Chem. Phys.*, *17*,  
1396 11227–11245, <https://doi.org/10.5194/acp-17-11227-2017>, 2017.

1397 DeMott, P. J., Prenni, A. J., McMeeking, G. R., Sullivan, R. C., Petters, M. D., Tobo, Y.,  
1398 Niemand, M., Möhler, O., Snider, J. R., Wang, Z., and Kreidenweis, S. M.: Integrating  
1399 laboratory and field data to quantify the immersion freezing ice nucleation activity of  
1400 mineral dust particles. *Atmospheric Chemistry and Physics*, *15*(1), 393-409.  
1401 <https://doi.org/10.5194/acp-15-393-2015>, 2015.

1402 DeMott, P. J., Mohler, O., Stetzer, O., Vali, G., Levin, Z., Petters, M. D., Murakami, M., Leisner,  
1403 T., Bundke, U., Klein, H., Kanji, Z. A., Cotton, R. Jones, H., Petters, M. D., Prenni, A.,  
1404 Benz, S. Brinkmann, M., Rzesanke, D., Saathoff, H. Nicolet, M., Gallavardin, S., Saito,  
1405 A., Nillius, B., Bingemer, H., Abbatt, J., Ardon, K., Ganor, E., Georgakopoulos, D. G.,  
1406 and Saunders, C.: Resurgence in ice nuclei measurement research. *Bulletin of the*  
1407 *American Meteorological Society*, *92*(12), 1623-+. <https://doi.org/10.1175/bams-d-10-3119.1>, 2011

1409 DeMott, P. J., Prenni, A. J., Liu, X., Kreidenweis, S. M., Petters, M. D., Twohy, C. H.,  
1410 Richardson, M. S., Eidhammer, T., Kreidenweis, S. M., and Rogers, D. C.: Predicting  
1411 global atmospheric ice nuclei distributions and their impacts on climate. *Proceedings of*  
1412 *the National Academy of Sciences of the United States of America*, *107*(25), 11217-  
1413 11222. <https://doi.org/10.1073/pnas.0910818107>,

1414 Durant, A. J., and Shaw, R. A.: Evaporation freezing by contact nucleation inside-out.  
1415 *Geophysical Research Letters*, *32*(20). <https://doi.org/10.1029/2005gl024175>, 2005.

1416 Eidhammer, T., DeMott, P. J., Prenni, A. J., Petters, M. D., Twohy, C. H., Rogers, D. C., Stith,  
1417 J., Heymsfield, A., Wang, Z., Haimov, S., French, J., Pratt, K., Prather, K., Murphy, S.,  
1418 Seinfeld, J., Subramanian, R. and Kreidenweis, S. M.: Ice initiation by aerosol particles:  
1419 Measured and predicted ice nuclei concentrations versus measured ice crystal  
1420 concentrations in an orographic wave cloud. *J. Atmos. Sci.*, *67*, 2417–2436.  
1421 <https://doi.org/10.1175/2010JAS3266.1>, 2010.

1422 Fornea, A. P., Brooks, S. D., Dooley, J. B., and Saha, A.: Heterogeneous freezing of ice on  
1423 atmospheric aerosols containing ash, soot, and soil. *Journal of Geophysical Research:*  
1424 *Atmospheres*, *114*(D13). <https://doi.org/10.1029/2009jd011958>, 2009.

1425 Froyd, K.D., Yu, P., Schill, G.P. *et al.* Dominant role of mineral dust in cirrus cloud formation  
1426 revealed by global-scale measurements. *Nat. Geosci.* **15**, 177–183.  
1427 <https://doi.org/10.1038/s41561-022-00901-w>, 2022.

1428 Froyd, K. D., Murphy, D. M., Brock, C. A., Campuzano-Jost, P., Dibb, J. E., Jimenez, J.-L.,  
1429 Kupc, A., Middlebrook, A. M., Schill, G. P., Thornhill, K. L., Williamson, C. J., Wilson,  
1430 J. C., and Ziemba, L. D.: A new method to quantify mineral dust and other aerosol  
1431 species from aircraft platforms using single-particle mass spectrometry. *Atmospheric*  
1432 *Measurement Techniques*, *12*(11), 6209-6239. <https://doi.org/10.5194/amt-12-6209-2019>,  
1433 2019.

1434 Gabey, A. M., Gallagher, M. W., Whitehead, J., Dorsey, J. R., Kaye, P. H., and Stanley, W. R.:  
1435 Measurements and comparison of primary biological aerosol above and below a tropical  
1436 forest canopy using a dual channel fluorescence spectrometer. *Atmospheric Chemistry*  
1437 *and Physics*, *10*(10), 4453-4466. <https://doi.org/10.5194/acp-10-4453-2010>, 2010.

1438 Garimella, S., Kristensen, T. B., Ignatius, K., Welti, A., Voigtländer, J., Kulkarni, G. R., Sagan,  
1439 F., Kok, G. L., Dorsey, J., Nichman, L., Rothenberg, D. A., Rösch, M., Kirchgäßner, A.



- 1440 C. R., Ladkin, R., Wex, H., Wilson, T. W., Ladino, L. A., Abbatt, J. P. D., Stetzer, O.,  
1441 Lohmann, U., Stratmann, F., and Cziczo, D. J.: The SPectrometer for Ice Nuclei (SPIN):  
1442 an instrument to investigate ice nucleation. *Atmospheric Measurement Techniques*, 9(7),  
1443 2781-2795. <https://doi.org/10.5194/amt-9-2781-2016>, 2016.
- 1444 Garimella, S., Rothenberg, D. A., Wolf, M. J., David, R. O., Kanji, Z. A., Wang, C., Rösch, M.,  
1445 and Cziczo, D. J.: Uncertainty in counting ice nucleating particles with continuous flow  
1446 diffusion chambers. *Atmospheric Chemistry and Physics*, 17(17), 10855-10864.  
1447 <https://doi.org/10.5194/acp-17-10855-2017>, 2017.
- 1448 Hader, J. D., Wright, T. P., & Petters, M. D.: Contribution of pollen to atmospheric ice nuclei  
1449 concentrations. *Atmospheric Chemistry and Physics*, 14(11), 5433-  
1450 5449. <https://doi.org/10.5194/acp-14-5433-2014>, 2014.
- 1451 Healy, D. A., Huffman, J. A., O'Connor, D. J., Pöhlker, C., Pöschl, U., & Sodeau, J. R.: Ambient  
1452 measurements of biological aerosol particles near Killarney, Ireland: a comparison  
1453 between real-time fluorescence and microscopy techniques. *Atmospheric Chemistry and  
1454 Physics*, 14(15), 8055-8069. <https://doi.org/10.5194/acp-14-8055-2014>, 2014.
- 1455 Hallar, A. G., G. Chirokova, I. McCubbin, T. H. Painter, C. Wiedinmyer, and C.  
1456 Dodson: Atmospheric bioaerosols transported via dust storms in the western United  
1457 States, *Geophys. Res. Lett.*, 38, L17801, <https://doi.org/10.1029/2011GL048166>, 2011.
- 1458 Healy, D. A., Huffman, J. A., O'Connor, D. J., Pöhlker, C., Pöschl, U., & Sodeau, J. R.: Ambient  
1459 measurements of biological aerosol particles near Killarney, Ireland: a comparison  
1460 between real-time fluorescence and microscopy techniques. *Atmospheric Chemistry and  
1461 Physics*, 14(15), 8055-8069. <https://doi.org/10.5194/acp-14-8055-2014>, 2014.
- 1462 Hiranuma, N., Augustin-Bauditz, S., Bingemer, H., Budke, C., Curtius, J., Danielczok, A., Diehl,  
1463 K., Dreischmeier, K., Ebert, M., Frank, F., Hoffmann, N., Kandler, K., Kiselev, A.,  
1464 Koop, T., Leisner, T., Möhler, O., Nillius, B., Peckhaus, A., Rose, D., Weinbruch, S.,  
1465 Wex, H., Boose, Y., DeMott, P. J., Hader, J. D., Hill, T. C. J., Kanji, Z. A., Kulkarni, G.,  
1466 Levin, E. J. T., McCluskey, C. S., Murakami, M., Murray, B. J., Niedermeier, D., Petters,  
1467 M. D., O'Sullivan, D., Saito, A., Schill, G. P., Tajiri, T., Tolbert, M. A., Welti, A., Whale,  
1468 T. F., Wright, T. P., and Yamashita, K.: A comprehensive laboratory study on the  
1469 immersion freezing behavior of illite NX particles: a comparison of 17 ice nucleation  
1470 measurement techniques, *Atmospheric Chemistry and Physics*, 15(5), 2489-2518.  
1471 <https://doi.org/10.5194/acp-15-2489-2015>, 2015.
- 1472 Huffman, J. A., Prenni, A. J., DeMott, P. J., Pöhlker, C., Mason, R. H., Robinson, N. H.,  
1473 Fröhlich-Nowoisky, J., Tobo, Y., Després, V. R., Garcia, E., Gochis, D. J., Harris, E.,  
1474 Müller-Germann, I., Ruzene, C., Schmer, B., Sinha, B., Day, D. A., Andreae, M. O.,  
1475 Jimenez, J. L., Gallagher, M., Kreidenweis, S. M., Bertram, A. K., and Pöschl, U.: High  
1476 concentrations of biological aerosol particles and ice nuclei during and after rain.  
1477 *Atmospheric Chemistry and Physics*, 13(13), 6151-6164. [https://doi.org/10.5194/acp-13-  
1478 6151-2013](https://doi.org/10.5194/acp-13-6151-2013), 2013.
- 1479 Jones, H. M., Flynn, M. J., DeMott, P. J., and Mohler, O.: Manchester Ice Nucleus Counter  
1480 (MINC) measurements from the 2007 International workshop on Comparing Ice  
1481 nucleation Measuring Systems (ICIS-2007). *Atmospheric Chemistry and Physics*, 11(1),  
1482 53-65. <https://doi.org/10.5194/acp-11-53-2011>, 2011.
- 1483 Kanji, Z. A., DeMott, P. J., Mohler, O., and Abbatt, J. P. D.: Results from the University of  
1484 Toronto continuous flow diffusion chamber at ICIS 2007: instrument intercomparison



- 1485 and ice onsets for different aerosol types. *Atmospheric Chemistry and Physics*, 11(1), 31-  
1486 41. <https://doi.org/10.5194/acp-11-31-2011>, 2011.
- 1487 Kanji, Z. A., Ladino, L. A., Wex, H., Boose, Y., Burkert-Kohn, M., Cziczó, D. J., & Krämer, M.:  
1488 Overview of Ice Nucleating Particles. In D. Baumgardner, G. M. McFarquhar, & A. J.  
1489 Heymsfield (Eds.), *Ice Formation and Evolution in Clouds and Precipitation:  
1490 Measurement and Modeling Challenges*, Meteorological Monographs, 58, 1.1-1.33.  
1491 <https://doi.org/10.1175/amsmonographs-d-16-0006.1>, 2017.
- 1492 Kaye, P. H., Stanley, W. R., Hirst, E., Foot, E. V., Baxter, K. L., and Barrington, S. J.: Single  
1493 particle multichannel bio-aerosol fluorescence sensor. *Optics Express*, 13(10), 3583-  
1494 3593. <https://doi.org/10.1364/OPEX.13.003583>, 2005.
- 1495 Knopf, D. A., Barry, K. R., Brubaker, T. A., Jahl, L. G., Jankowski, K. A. L., Li, J., Lu, Y.,  
1496 Monroe, L. W., Moore, K. A., Rivera-Adorno, F. A., Saucedo, K. A., Shi, Y., Tomlin, J.  
1497 M., Vepuri, H. S. K., Wang, P., Lata, N. N., Levin, E. J. T., Creamean, J. M., Hill, T. C.  
1498 J., China, S., Alpert, P. A., Moffet, R. C., Hiranuma, N., Sullivan, R. C., Fridlind, A. M.,  
1499 West, M., Riemer, N., Laskin, A., DeMott, P. J., & Liu, X. (2021). Aerosol–Ice  
1500 Formation Closure: A Southern Great Plains Field Campaign, *Bulletin of the American  
1501 Meteorological Society*, 102(10), E1952-E197, [https://doi.org/10.1175/BAMS-D-20-  
0151.1](https://doi.org/10.1175/BAMS-D-20-<br/>1502 0151.1)
- 1503 Kulkarni, G. and Kok, G (2012).: Mobile Ice Nucleus Spectrometer, Pacific Northwest National  
1504 Laboratory, Richland, WA, 13 pg.
- 1505 Lacher, L., Adams, M. P., Barry, K., Bertozzi, B., Bingemer, H., Boffo, C., Bras, Y., Büttner, N.,  
1506 Castarede, D., Cziczó, D. J., DeMott, P. J., Fösig, R., Goodell, M., Höhler, K., Hill, T. C.  
1507 J., Jentsch, C., Ladino, L. A., Levin, E. J. T., Mertes, S., Möhler, O., Moore, K. A.,  
1508 Murray, B. J., Nadolny, J., Pfeuffer, T., Picard, D., Ramírez-Romero, C., Ribeiro, M.,  
1509 Richter, S., Schrod, J., Sellegri, K., Stratmann, F., Swanson, B. E., Thomson, E., Wex,  
1510 H., Wolf, M., and Freney, E.: The Puy de Dôme ICe Nucleation Intercomparison  
1511 Campaign (PICNIC): Comparison between online and offline methods in ambient air,  
1512 *Atmos. Chem. Phys.*, 24, 2651–2678, <https://doi.org/10.5194/acp-24-2651-2024>, 2024.
- 1513 Levin, E. J. T., DeMott, P. J., Suski, K. J., Boose, Y., Hill, T. C. J., McCluskey, C. S., Schill, G.  
1514 P., Rocci, K., Al-Mashat, H., Kristensen, L. J., Cornwell, G. C., Prather, K. A.,  
1515 Tomlinson, J. M., Mei, F., Hubbe, J., Pekour, M. S., Sullivan, R. J., Leung L. R., and  
1516 Kreidenweis, S. M.: Characteristics of ice nucleating particles in and around California  
1517 winter storms, *Journal of Geophysical Research: Atmospheres*, 124, 11,530-11,551,  
1518 <https://doi.org/10.1029/2019JD030831>, 2019.
- 1519 Lohmann, U., and Feichter, J.: Global indirect aerosol effects: a review. *Atmospheric Chemistry  
1520 and Physics*, 5, 715-737. <https://doi.org/10.5194/acp-5-715-2005>, 2005.
- 1521 Marcolli, C., Deposition nucleation viewed as homogeneous or immersion freezing in pores and  
1522 cavities. *Atmospheric Chemistry and Physics*, 14(4), 2071-2104.  
1523 <https://doi.org/10.5194/acp-14-2071-2014>, 2014.
- 1524 Mason, R. H., Si, M., Chou, C., Irish, V. E., Dickie, R., Elizondo, P., Wong, R., Brintnell, M.,  
1525 Elsasser, M., Lassar, W. M., Pierce, K. M., Leitch, W. R., MacDonald, A. M., Platt, A.,  
1526 Toom-Saunty, D., Sarda-Estève, R., Schiller, C. L., Suski, K. J., Hill, T. C. J., Abbatt, J.  
1527 P. D., Huffman, J. A., DeMott, P. J., and Bertram, A. K.: Size-resolved measurements of  
1528 ice-nucleating particles at six locations in North America and one in Europe, *Atmos.  
1529 Chem. Phys.*, 16, 1637–1651, <https://doi.org/10.5194/acp-16-1637-2016>, 2016.



- 1530 McCluskey, C. S., Gettelman, A., Bardeen, C. G., DeMott, P. J., Moore, K. A., Kreidenweis, S.  
1531 M., Hill, T. C. J., Barry, K. R., Twohy, C. H., Toohey, D. W., Rainwater, B., Jensen, J.  
1532 B., Reeves, J. M., Alexander, S. P. and McFarquhar, G. M.: Simulating Southern Ocean  
1533 aerosol and ice nucleating particles in the Community Earth System Model version 2.  
1534 *Journal of Geophysical Research: Atmospheres*, 128, e2022JD036955, 2023.  
1535 <https://doi.org/10.1029/2022JD036955>, 2023.
- 1536 McCluskey, C. S., Hill, T. C. J., Humphries, R. S., Rauker, A. M., Moreau, S., Stratton, P. G.,  
1537 Chambers, S. D., Williams, A. G., McRobert, I., Ward, J., Keywood, M. D., Harnwell,  
1538 J., Ponsonby, W., Loh, Z.M., Krummel, P. B., Protat, A., Kreidenweis, S.M., and  
1539 DeMott, P. J.: Observations of ice nucleating particles over Southern Ocean waters.  
1540 *Geophysical Research Letters*, 45, 11,989–11,997,  
1541 <https://doi.org/10.1029/2018GL079981>, 2018.
- 1542 Möhler, O., Adams, M., Lacher, L., Vogel, F., Nádolny, J., Ullrich, R., Boffo, C., Pfeuffer, T.,  
1543 Hobl, A., Weiß, M., Vepuri, H. S. K., Hiranuma, N., and Murray, B. J.: The Portable Ice  
1544 Nucleation Experiment (PINE): a new online instrument for laboratory studies and  
1545 automated long-term field observations of ice-nucleating particles. *Atmospheric*  
1546 *Measurement Techniques*, 14(2), 1143-1166. <https://doi.org/10.5194/amt-14-1143-2021>,  
1547 2021.
- 1548 Morris, C. E., Sands, D. C., Bardin, M., Jaenicke, R., Vogel, B., Leyronas, C., Ariya, P. A., and  
1549 Psenner, R.: Microbiology and atmospheric processes: research challenges concerning  
1550 the impact of airborne micro-organisms on the atmosphere and climate. *Biogeosciences*,  
1551 8, 17. <https://doi.org/10.5194/bg-8-17-2011>, 2011.
- 1552 Murray, B. J., O'Sullivan, D., Atkinson, J. D., & Webb, M. E: Ice nucleation by particles  
1553 immersed in supercooled cloud droplets. *Chemical Society Reviews*, 41(19), 6519-6554.  
1554 <https://doi.org/10.1039/C2CS35200A>, 2012.
- 1555 Niemand, M., Mohler, O., Vogel, B., Vogel, H., Hoose, C., Connolly, P., Klein, H. Bingemer,  
1556 H., DeMott, P. J., Skrotzki, J., and Leisner, T.: A Particle-Surface-Area-Based  
1557 Parameterization of Immersion Freezing on Desert Dust Particles. *Journal of the*  
1558 *Atmospheric Sciences*, 69(10), 3077-3092. <https://doi.org/10.1175/jas-d-11-0249.1>, 2012.
- 1559 Perring, A. E., Schwarz, J. P., Baumgardner, D., Hernandez, M. T., Spracklen, D. V., Heald, C.  
1560 L., Gao, R. S., Kok, G., McMeeking, G. R., McQuaid, J. B., and Fahey, D. W.:  
1561 Airborne observations of regional variation in fluorescent aerosol across the United  
1562 States. *Journal of Geophysical Research-Atmospheres*, 120(3), 1153-1170.  
1563 <https://doi.org/10.1002/2014jd022495>, 2015.
- 1564 Petersen, R. C., Hallar, A. G., McCubbin, I. B., Ogren, J. A., Andrews, E., Lowenthal, D.,  
1565 Gorder, R., Purcell, R., Sleeth, D., and Novoselov, I.: Numerical, wind-tunnel, and  
1566 atmospheric evaluation of a turbulent ground-based inlet sampling system, *Aerosol*  
1567 *Science and Technology*, 53 (6), 712-727,  
1568 <https://doi.org/10.1080/02786826.2019.1602718>, 2019.
- 1569 Petters, M. D., and Wright, T. P.: Revisiting ice nucleation from precipitation samples.  
1570 *Geophysical Research Letters*, 42(20), 8758-8766. doi:10.1002/2015gl065733, 2015.
- 1571 Pöhlker, C., Huffman, J. A., and Pöschl, U.: Autofluorescence of atmospheric bioaerosols –  
1572 fluorescent biomolecules and potential interferences. *Atmospheric Measurement*  
1573 *Techniques*, 5(1), 37-71. <https://doi.org/10.5194/amt-5-37-2012>, 2012.





- 1574 Rogers, D.C.: Development of a continuous flow thermal gradient diffusion chamber for ice  
1575 nucleation studies. *Atmos. Res.*, 22, 149-181, [https://doi.org/10.1016/0169-](https://doi.org/10.1016/0169-8095(88)90005-1)  
1576 [8095\(88\)90005-1](https://doi.org/10.1016/0169-8095(88)90005-1), 1988.
- 1577 Rogers, D. C., DeMott, P. J., Kreidenweis S. M., and Chen, Y.: A continuous flow diffusion  
1578 chamber for airborne measurements of ice nuclei, *J. Atmos. Oceanic Technol.*, 18, 725-  
1579 741, [https://doi.org/10.1175/1520-0426\(2001\)018<0725:ACFDCF>2.0.CO;2](https://doi.org/10.1175/1520-0426(2001)018<0725:ACFDCF>2.0.CO;2), 2001.
- 1580 Schill, G. P., DeMott, P. J., Emerson, E. W., Rauker, A. M. C., Kodros, J. K., Suski, K. J., Hill,  
1581 T. C. J., Levin, E. J. T., Pierce, J. R., Farmer, D. K., and Kreidenweis, S. M.: The  
1582 contribution of black carbon to global ice nucleating particle concentrations relevant to  
1583 mixed-phase clouds. *Proceedings of the National Academy of Sciences*, 117 (37), 22705–  
1584 22711, <https://doi.org/10.1073/pnas.2001674117>, 2020.
- 1585 Schrod, J., Danielczok, A., Weber, D., Ebert, M., Thomson, E. S., and Bingemer, H. G.: Re-  
1586 evaluating the Frankfurt isothermal static diffusion chamber for ice nucleation, *Atmos.*  
1587 *Meas. Tech.*, 9, 1313–1324, <https://doi.org/10.5194/amt-9-1313-2016>, 2016.
- 1588 Schrod, J., Thomson, E. S., Weber, D., Kossmann, J., Pöhlker, C., Saturno, J., Ditas, F., Artaxo,  
1589 P., Clouard, V., Saurel, J.-M., Ebert, M., Curtius, J., and Bingemer, H. G.: Long-term  
1590 deposition and condensation ice-nucleating particle measurements from four stations  
1591 across the globe, *Atmos. Chem. Phys.*, 20, 15983–16006, [https://doi.org/10.5194/acp-20-](https://doi.org/10.5194/acp-20-15983-2020)  
1592 [15983-2020](https://doi.org/10.5194/acp-20-15983-2020), 2020.
- 1593 Seifert, P., Ansmann, A., Groß, S., Freudenthaler, V., Heinold, B., Hiebsch, A., Mattis, I.,  
1594 Schmidt, J., Schnell, F., Tesche, M., Wandinger, U., and Wiegner, M.: Ice formation in  
1595 ash-influenced clouds after the eruption of the Eyjafjallajökull volcano in April 2010.  
1596 *Journal of Geophysical Research: Atmospheres*, 116(D20).  
1597 <https://doi.org/10.1029/2011jd015702>, 2011.
- 1598 Suski, K. J., Hill, T. C. J., Levin, E. J. T., Miller, A., DeMott, P. J., and Kreidenweis, S. M.: Agricultural  
1599 harvesting emissions of ice-nucleating particles, *Atmos. Chem. Phys.*, 18, 13755-13771,  
1600 <https://doi.org/10.5194/acp-18-13755-2018>.
- 1601 Testa, B., Hill, T. C. J., Marsden, N. A., Barry, K. R., Hume, C. C., Bian, Q., Uetake, J., Hare,  
1602 H., Perkins, R. J., Möhler, O., Kreidenweis, S. M. and DeMott, P. J.: Ice nucleating  
1603 particles in the boundary layer of the Sierras de Córdoba, Argentina, during the Cloud,  
1604 Aerosol, and Complex Terrain Interactions experiment, *Journal of Geophysical*  
1605 *Research: Atmospheres* 126, e2021JD03518, <https://doi.org/10.1029/2021JD035186>,  
1606 2021.
- 1607 Tobo, Y., DeMott, P. J., Hill, T. C. J., Prenni, A. J., Swoboda-Colberg, N. G., Franc, G. C., and  
1608 Kreidenweis, S. M.: Organic matter matters for ice nuclei of agricultural soil origin.  
1609 *Atmos. Chem. Phys.*, 14, 8521–8531, <https://doi.org/10.5194/acp-14-8521-2014>, 2014.
- 1610 Tobo, Y., Prenni, A. J., DeMott, P. J., Huffman, J. A., McCluskey, C. S., Tian, G. X., Pöhlker,  
1611 C., Pöschl, U., and Kreidenweis, S. M.: Biological aerosol particles as a key determinant  
1612 of ice nuclei populations in a forest ecosystem. *Journal of Geophysical Research-*  
1613 *Atmospheres*, 118(17), 10100-10110. <https://doi.org/10.1002/jgrd.50801>, 2013.
- 1614 Ullrich, R., Hoose, C., Möhler, O., Niemand, M., Wagner, R., Höhler, K., Hiranuma, N.,  
1615 Saathoff, H., and Leisner, T.: A New Ice Nucleation Active Site Parameterization for  
1616 Desert Dust and Soot. *Journal of the Atmospheric Sciences*, 74(3), 699-717.  
1617 <https://doi.org/10.1175/jas-d-16-0074.1>, 2017.



- 1618 Willeke, K., Lin, X., and Grinshpun, S. A.: Improved Aerosol Collection by Combined  
1619 Impaction and Centrifugal Motion, *Aerosol. Sci. Tech.*, 28(5), 439–456.  
1620 <https://doi.org/10.1080/02786829808965536>, 1998.
- 1621 Wright, T. P., & Petters, M. D.: The role of time in heterogeneous freezing nucleation. *Journal of*  
1622 *Geophysical Research: Atmospheres*, 118, 3731–3743.  
1623 <https://doi.org/10.1002/jgrd.503652013>, 2013.
- 1624 Wright, T. P., Hader, J. D., McMeeking, G. R., and Petters, M.D.: High Relative Humidity as a  
1625 Trigger for Widespread Release of Ice Nuclei, *Aerosol Science and Technology*, 48 (11),  
1626 i-v. <https://doi.org/10.1080/02786826.2014.968244>, 2014.
- 1627 Wright, T. P., Petters, M. D., Hader, J. D., Morton, T., & Holder, A. L.: Minimal cooling rate  
1628 dependence of ice nuclei activity in the immersion mode. *Journal of Geophysical*  
1629 *Research: Atmospheres*, 118, 10,535–10,543. <https://doi.org/10.1002/jgrd.50810>, 2013.
- 1630 Vali, G., DeMott, P. J., Möhler, O. and Whale, T. F.: Technical Note: A proposal for ice nucleation  
1631 terminology, *Atmos. Chem. Phys.*, 15, 10263–10270, <https://doi.org/10.5194/acp-15-10263-2015>,  
1632 2015.
- 1633 Vali, G.: Nucleation terminology. *Journal of Aerosol Science*, 16(6), 575-576,  
1634 [https://doi.org/10.1016/0021-8502\(85\)90009-6](https://doi.org/10.1016/0021-8502(85)90009-6), 1985.
- 1635 Vali, G.: Quantitative evaluation of experimental results on the heterogeneous freezing  
1636 nucleation of supercooled liquids. *J. Atmos. Sci.*, 28, 402–409,  
1637 [https://doi.org/10.1175/1520-0469\(1971\)028<0402:QEOERA>2.0.CO;2](https://doi.org/10.1175/1520-0469(1971)028<0402:QEOERA>2.0.CO;2), 1971.
- 1638 Wagner, R., Kiselev, A., Mohler, O., Saathoff, H., & Steinke, I.: Pre-activation of ice-nucleating  
1639 particles by the pore condensation and freezing mechanism. *Atmospheric Chemistry and*  
1640 *Physics*, 16(4), 2025-2042. <https://doi.org/10.5194/acp-16-2025-2016>, 2016.
- 1641 Wex, H., Augustin-Bauditz, S., Boose, Y., Budke, C., Curtius, J., Diehl, K., Dreyer, A., Frank,  
1642 F., Hartmann, S., Hiranuma, N., Jantsch, E., Kanji, Z. A., Kiselev, A., Koop, T., Möhler,  
1643 O., Niedermeier, D., Nillius, B., Rösch, M., Rose, D., Schmidt, C., Steinke, I., and  
1644 Stratmann, F.: Intercomparing different devices for the investigation of ice nucleating  
1645 particles using Snomax (R) as test substance. *Atmospheric Chemistry and Physics*, 15(3),  
1646 1463-1485. <https://doi.org/10.5194/acp-15-1463-2015>, 2015.
- 1647 Willeke, K., Lin, X., and Grinshpun, S. A.: Improved Aerosol Collection by Combined  
1648 Impaction and Centrifugal Motion, *Aerosol. Sci. Tech.*, 28(5), 439–456.  
1649 <https://doi.org/10.1080/02786829808965536>, 1998.
- 1650 Wright, T. P., & Petters, M. D.: The role of time in heterogeneous freezing nucleation. *Journal of*  
1651 *Geophysical Research: Atmospheres*, 118, 3731–3743.  
1652 <https://doi.org/10.1002/jgrd.503652013>, 2013.
- 1653 Wright, T. P., Hader, J. D., McMeeking, G. R., and Petters, M.D.: High Relative Humidity as a  
1654 Trigger for Widespread Release of Ice Nuclei, *Aerosol Science and Technology*, 48 (11),  
1655 i-v. <https://doi.org/10.1080/02786826.2014.968244>, 2014.
- 1656 Wright, T. P., Petters, M. D., Hader, J. D., Morton, T., & Holder, A. L.: Minimal cooling rate  
1657 dependence of ice nuclei activity in the immersion mode. *Journal of Geophysical*  
1658 *Research: Atmospheres*, 118, 10,535–10,543. <https://doi.org/10.1002/jgrd.50810>, 2013.
- 1659 Yadav, S., Venezia, R. E., Paerl, R. W., & Petters, M. D.: Characterization of ice-nucleating  
1660 particles over Northern India. *Journal of Geophysical Research:*  
1661 *Atmospheres*, 124, 10467–10482. <https://doi.org/10.1029/2019JD030702>, 2019.
- 1662 Zawadowicz, M. A., Froyd, K. D., Murphy, D. M., and Cziczo, D. J.: Improved identification of  
1663 primary biological aerosol particles using single-particle mass spectrometry. *Atmospheric*



- 1664            *Chemistry and Physics*, 17(11), 7193-7212. <https://doi.org/10.5194/acp-17-7193-2017>,  
1665            2017.
- 1666        Zawadowicz, M. A., Froyd, K. D., Perring, A. E., Murphy, D. M., Spracklen, D. V., Heald, C.  
1667            L., Buseck, P. R., and Cziczo, D. J.: Model-measurement consistency and limits of  
1668            bioaerosol abundance over the continental United States. *Atmospheric Chemistry and*  
1669            *Physics*, 19(22), 13859-13870. <https://doi.org/10.5194/acp-19-13859-2019>, 2019.
- 1670        Zenker, J., Collier, K. N., Xu, G., Yang, P., Levin, E. J. T., Suski, K. J., DeMott, P. J., and  
1671            Brooks, S. D.: Using depolarization to quantify ice nucleating particle concentrations: a  
1672            new method, *Atmos. Meas. Tech.*, 10, 4639–4657, [https://doi.org/10.5194/amt-10-4639-](https://doi.org/10.5194/amt-10-4639-2017)  
1673            [2017](https://doi.org/10.5194/amt-10-4639-2017), 2017.
- 1674
- 1675